

In vivo efficacy of an injectable piezoelectric nanocomposite hydrogel and low-intensity pulsed ultrasound in two preclinical models of osteoarthritis

Matilde Tschon^{a, b}, Giorgia Codispoti^{a, b}, Paolo Cabras^{b, c}, Andrea Cafarelli^{d, e},
Diego Trucco^{d, e}, Lorenzo Vannozzi^{d, e}, Cristina Manferdini^f, Melania Carniato^{a, b},
Giorgio Cassiolas^{a, b}, Lucia Martini^a, Milena Fini^g, Giovanni D'Atri^f, Carsten Jost^h,
Yirij Fedutik^h, Gilbert Daniel Nessimⁱ, Erik Dumont^b, Gina Lisignoli^{f, *}, Leonardo Ricotti^{d, e, **}

^a IRCCS Istituto Ortopedico Rizzoli, Struttura Complessa Scienze e Tecnologie Chirurgiche, 40136, Bologna, Italy

^b Image Guided Therapy, Pessac, France

^c Université de Strasbourg, CNRS, INSERM, ICube, UMR7357, Strasbourg, France

^d The BioRobotics Institute, Scuola Superiore Sant'Anna, 56127, Pisa, Italy

^e Department of Excellence in Robotics & AI, Scuola Superiore Sant'Anna, 56127, Pisa, Italy

^f IRCCS Istituto Ortopedico Rizzoli, Laboratorio di Immunoreumatologia e Rigenerazione Tissutale, 40136, Bologna, Italy

^g IRCCS Istituto Ortopedico Rizzoli, Scientific Director, 40136, Bologna, Italy

^h PlasmaChem GmbH, Schwarzschildstraße 10, 12489, Berlin, Germany

ⁱ Department of Chemistry and Institute of Nanotechnology, Bar-Ilan University, Ramat Gan, 52900, Israel

ARTICLE INFO

Keywords:

Osteoarthritis
Rabbit and sheep models
Ultrasound
Cartilage regeneration
Mesenchymal stromal cell
Piezoelectric hydrogel

ABSTRACT

Smart hydrogels embedding mesenchymal stromal cells are receiving increasing attention as a potential solution for preventing articular cartilage degeneration in knee osteoarthritis (OA). In this work we demonstrate that an injectable piezoelectric hydrogel embedding autologous adipose tissue-derived mesenchymal stromal cells (ASCs), stimulated by low-intensity pulsed ultrasound (LIPUS), is effective in reducing knee OA in two preclinical surgically induced OA models. A medium-sized rabbit model was used to evaluate sex differences in treatment efficacy, while a large-sized sheep model was employed to assess the translatability of this innovative approach to a scenario with similarities to human conditions. We developed computational models to ensure reliable and precise delivery of a specific ultrasound dose to the target, modelling wave propagation through tissues and considering the anatomy of the two experimental animal models. Sex-based differences in therapy effectiveness were observed in rabbits, with better macroscopic and microscopic outcomes in counteracting OA in female animals. Furthermore, we found that the combination of ASC-laden piezoelectric hydrogel and LIPUS can be scaled in a large-sized sheep model, proving effective in counteracting OA.

1. Introduction

Osteoarthritis (OA) is the most common progressive musculoskeletal disease affecting multiple joints [1]. Its incidence increases with age, particularly affecting women, leading to high costs for individuals, the healthcare system, and society at large [2]. Due to various factors such as mechanical overload, inflammation, hormonal fluctuations, body weight, aging, and lifestyle, the knee is the most frequently affected joint, with a prevalence of 365 million people worldwide [3]. The pathogenesis of OA involves several stages that correspond to the

clinical progression of the disease [4]. In the early stages, an inflammatory process begins in the synovial membrane. As the disease progresses, structural changes occur in the different layers of the cartilage. Initially, chondrocytes undergo hypertrophy, which ultimately leads to their degeneration. This results in cartilage erosion, followed by exposure and sclerosis of the subchondral bone in the later stages [5]. The Osteoarthritis Research Society International (OARSI) guidelines recommended that patients with early-stage knee OA (KOA) who do not have evident cartilage lesions should first adopt non-pharmacological approaches [6,7]. However, these conservative strategies are poorly

* Corresponding author.

** Corresponding author. The BioRobotics Institute, Scuola Superiore Sant'Anna, 56127 Pisa, Italy.

E-mail addresses: gina.lisignoli@ior.it (G. Lisignoli), leonardo.ricotti@santannapisa.it (L. Ricotti).

<https://doi.org/10.1016/j.biomaterials.2025.123728>

Received 12 May 2025; Received in revised form 18 September 2025; Accepted 19 September 2025

Available online 20 September 2025

0142-9612/© 2025 The Authors. Published by Elsevier Ltd. This is an open access article under the CC BY license (<http://creativecommons.org/licenses/by/4.0/>).

effective in slowing down the degeneration process [8]. In advanced KOA, the administration of viscosupplements and pharmacological therapies, mainly consisting of non-steroidal anti-inflammatory drugs (NSAIDs), *cyclooxygenase-2* (COX-2) inhibitors, analgesics, or intra-articular corticosteroids, is recommended before considering surgical management [9]. Despite numerous pharmacological and non-pharmacological strategies have been proposed to alleviate symptoms and slow down the progression of the disease, there are currently no effective long-term therapies available for KOA [10,11].

In recent years, several tissue engineering and regenerative medicine approaches have been pursued to counteract articular cartilage degeneration in KOA [12,13]. The development of tissue-engineered constructs, consisting of synthetic or natural biomaterials and stromal cells to promote cell viability and chondrogenic differentiation, represents an exciting perspective [14]. However, the solutions developed over the past few decades have shown limited efficacy [15–18] in cartilage regeneration, mainly due to the biological properties of the regenerated cartilage, which still require optimization to ensure safe and effective therapies. Additionally, other factors such as the selection of appropriate cell sources, biomaterials, and the application of suitable biochemical, mechanical and biological stimuli contribute to hindering widespread clinical translation.

Alternative therapeutic strategies have also been explored, including the use of biophysical stimulation techniques such as electric, electromagnetic fields, as well as ultrasound [19–21]. However, the clinical outcomes reported so far remain controversial. Among the various forms of physical energy employed, low-intensity pulsed ultrasound (LIPUS) has a stimulation regimen characterized by intrinsically safe, low-energy pressure waves transmitted in a pulsed mode to minimize the temperature increase in tissues. At the cellular level, ultrasound waves stimulate specific mechano-receptors on the cell membrane, activating intracellular pathways that promote regenerative processes [22] and modulate inflammation [23]. LIPUS is currently approved by the Food and Drug Administration (FDA) for fracture healing [24]. Positive therapeutic effects have also been demonstrated *in vitro* and *in vivo* on various tissue types, although further optimization of the procedures and a deeper understanding of the underlying mechanisms are still needed. Recent studies have shown various beneficial biological effects (e.g., neural modulation, cell proliferation or inhibition, and stromal cell differentiation) triggered by the combined use of ultrasound and responsive piezoelectric nanoparticles [25,26]. This has led to growing scientific interest in using piezoelectric nanoparticles as nano transducers for indirect electrical stimulation at the cellular and tissue levels.

A recent research trend has emerged that exploits piezoelectric biomaterials and nanocomposite hydrogels for osteoarticular tissue regeneration [27,28]. Our previous work demonstrated that a two-component bio-instructive polymeric matrix (VitroGel-RGD®, VG-RGD), doped with smart nanomaterials, namely piezoelectric barium titanate nanoparticles (BTNPs) and graphene oxide (GO) nanoflakes, promoted the chondrogenic differentiation of adipose-derived stromal cells (ASCs) and counteracted inflammation, *in vitro* [22,29]. Through proteomic analyses we demonstrated the mechanisms responsible for the ASCs' response to the generated piezopotential *in vitro*, revealing that LIPUS stimulation influenced various biological processes involved in mechanotransduction. LIPUS induced an enrichment of proteins involved in cytoskeleton and extracellular matrix organization, collagen fibril organization, as well as specific signalling pathways such as non-canonical Wnt pathway, which regulates the cytoskeleton, and integrin-mediated signalling, which is involved in the chondrogenic commitment of ASCs [22].

These effects were achieved by stimulating the nanocomposite (Nanocomp) hydrogel with a precise dose (1 MHz, 250 mW/cm²) of LIPUS, which activated the piezoelectric nanomaterials, generating an intracellular electric field that drove chondrogenic differentiation. The preclinical biocompatibility of Nanocomp, performed according to ISO 10993 standards, was also evaluated, demonstrating its safety. These

findings supported the hypothesis that such a new strategy may overcome the limitations of existing clinical approaches, by promoting cartilage regeneration even in an inflammatory milieu.

Starting from these promising results, we hypothesized that this therapy, based on VG-RGD hydrogel, BTNPs and GO nanomaterials, ASCs and LIPUS biophysical stimulation, could be effective in treating and slowing down the progression of KOA *in vivo*. To test this hypothesis, we developed computational models of the ultrasound wave propagation through tissues based on the anatomy of the two experimental animal models involved in the study: medium-sized rabbit and large-sized sheep models of KOA. Then, we treated both OA animal models with the above-mentioned therapeutic solution and evaluated the effects in terms of histological, histomorphometric and synovial fluid analyses. Sex-related differences were also assessed for the rabbit model, along with the presence of any Titanium and Barium residuals from BTNPs, using inductively coupled plasma mass spectrometry (ICP-MS). A depiction of the workflow is summarized in Scheme 1.

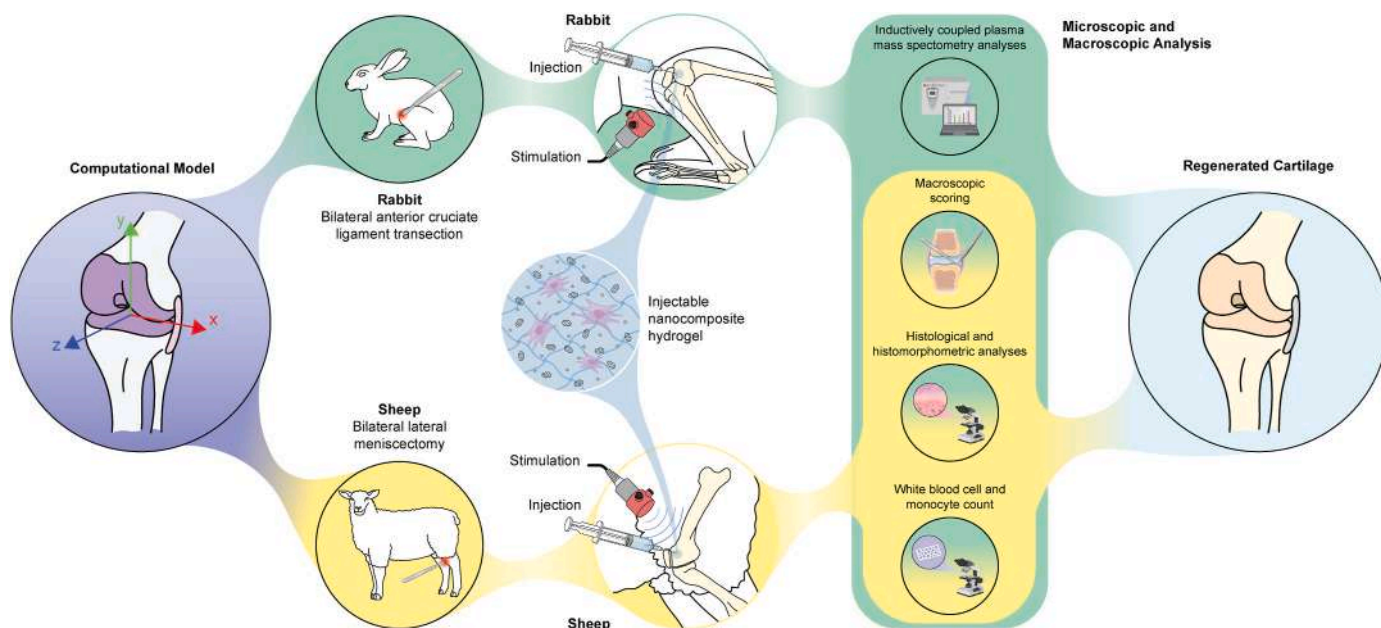
2. Results

2.1. Computational models for *in vivo* ultrasound stimulation

As discussed in Cafarelli et al. [25] and experimentally demonstrated by Ricotti et al. [22], the effectiveness of the proposed approach in this field strongly depends on the applied LIPUS stimulation protocol and the reliability/consistency of the obtained results. These factors are primarily driven by the ability to control the correct dose of mechanical energy at the target. This aspect is often overlooked in *in vitro* studies focused on LIPUS [30,31], but *ad hoc* set-ups can allow overcoming this challenge [32]. The scientific community has increasingly adopted such a dose-controlled approach for *in vitro* experiments in recent years. However, even if the ultrasound dose is correctly evaluated and managed *in vitro*, delivering it reliably and consistently *in vivo* presents additional challenges [25]. Indeed, *in vivo*, the complexity of the anatomy and the presence of multiple tissue interfaces make it difficult to estimate and control the pressure field acting on the region of interest. *In vivo*, reflections, attenuations, diffractions, and other physical phenomena can affect and distort the ultrasound beam, potentially reducing the efficacy of the stimulation. To address this, we utilized acoustic simulations tailored to the specific anatomy of the animal to investigate the propagation of ultrasound waves through the tissues. This allowed us to identify the optimal experimental set-up (in terms of transducer positioning and source power) to reproduce, *in vivo*, the same stimulation conditions shown to be effective *in vitro* [22] (target *in situ* intensity of 250 mW/cm², pulse repetition frequency of 1 kHz, stimulation frequency 1 MHz). To better define the translatability of the selected LIPUS *in vitro* parameters into *in vivo* models, two preclinical surgically-induced OA models of different sizes were selected: a medium-sized rabbit model and a large-sized sheep model.

For the rabbit model, a three-dimensional (3D) model of rabbit anatomy was reconstructed from a micro computed tomography (CT) scan of an *ex-vivo* knee of a New Zealand rabbit. 3D Slicer tools were used to segment the main tissues within the targeted area (Fig. 1 a) and reconstruct the 3D model of the rabbit knee, as well as define the region of interest (ROI), the area on the condyles where the therapy should be performed (Fig. 1 b). The best transducer position was determined based on the *uniformity score*, defined as the percentage of voxels stimulated at the target intensity (i.e., 250 mW/cm² with a tolerance of $\pm 30\%$). The transducer (visualized as a disc, as shown in Fig. 1 c) was positioned at 45° with respect to the tibial plateau (espousing the skin surface), at 20 mm from the skin (30 mm from the condyles) and centered with respect to the femur in the medio-lateral direction. The resulting normalized pressure distribution in space is shown in Fig. 1 c.

The *attenuation factor* (calculated as the ratio between the median value of the simulated pressure within the animal model condyle ROI and the median value of the simulated pressure distribution



Scheme 1. Workflow of the activities performed starting from the computational model of knee rabbits and sheep to test the therapeutic solution in two OA animal models.

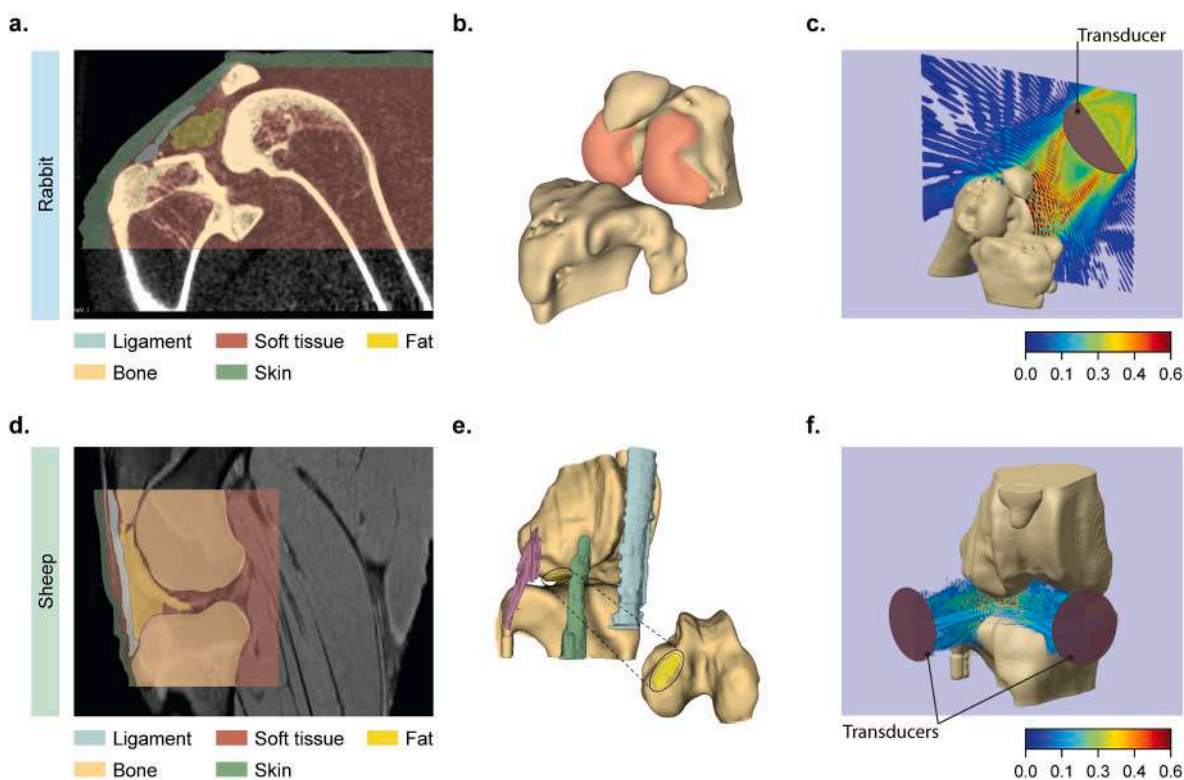


Fig. 1. Computational model driving the optimization of ultrasound stimulation *in vivo* for rabbit (first row) and sheep (second row). (a) anatomical CT images of the rabbit knee and different tissue segmentation, (b) 3D model of the knee joint and corresponding target ROI (in red) for the rabbit, (d) Anatomical MR image of the sheep knee and different tissue segmentation, (e) 3D model of the sheep knee with bone (light brown), latero-collateral ligament (purple) patellar ligament (light blue), long digital extensor (green) and target ROI for treatment (vivid purple), (c) and (f) stimulation scenario and corresponding normalized (from 0 to 1) pressure map overlaid on the bone model for rabbit and sheep, respectively. For the sake of clarity, only the bone is shown. (For interpretation of the references to color in this figure legend, the reader is referred to the Web version of this article.)

theoretically acting on the hydrogel sample in the *in vitro* set-up) was 0.83.

Based on this factor, the transducer driving system was set to achieve an intensity of 348 mW/cm² in the free field, compensating for acoustic

losses (due to tissue interaction) and ensuring that the target received the desired intensity of 250 mW/cm².

To determine how the set-up configuration influenced stimulation efficiency and repeatability, several scenarios were considered by

modifying one parameter at a time: distance from the skin (and condyle), medio-lateral alignment and transducer orientation (defined as the angle with respect to the tibial plateau surface). The distance (Fig. S1) and the orientation (Fig. S2) of the transducer did not significantly affect the overall stimulation at the target. However, particular attention had to be paid to the medio-lateral alignment (Fig. S3) as a small displacement could result in partial stimulation of one of the condyles (Figs. S3 b and c).

For the sheep model, the 3D model was reconstructed from magnetic resonance (MR) images of an *ex-vivo* knee of an adult cross-bred sheep (Fig. 1 d). After segmentation, the model was resampled into isometric voxels of 0.21 mm (corresponding to approximately 7 points per wavelength) to enhance the MR image's original resolution (0.5 mm).

The primary challenge with this model was that the target area was partially obscured by the long digital extensor (LDE, green structure in Fig. 1 e). Indeed, the acoustic attenuation of these structures was quite significant (around 14.5 Np/m, at 1 MHz).

Several simulations were performed to identify the best acoustic window for stimulating the targeted region. The optimal set-up, in terms of *uniformity score* was selected (Fig. 1 f, light violet disc on the left, the one directed to the lateral condyle region). Due to the joint dimensions, a second transducer was added to stimulate a larger volume within the joint (Fig. 1 f, violet disc on the right).

For this configuration, the uniformity score and attenuation factor were estimated from simulation results as 25.2 % and 1.08, respectively. The attenuation factor was slightly higher than 1, likely due to

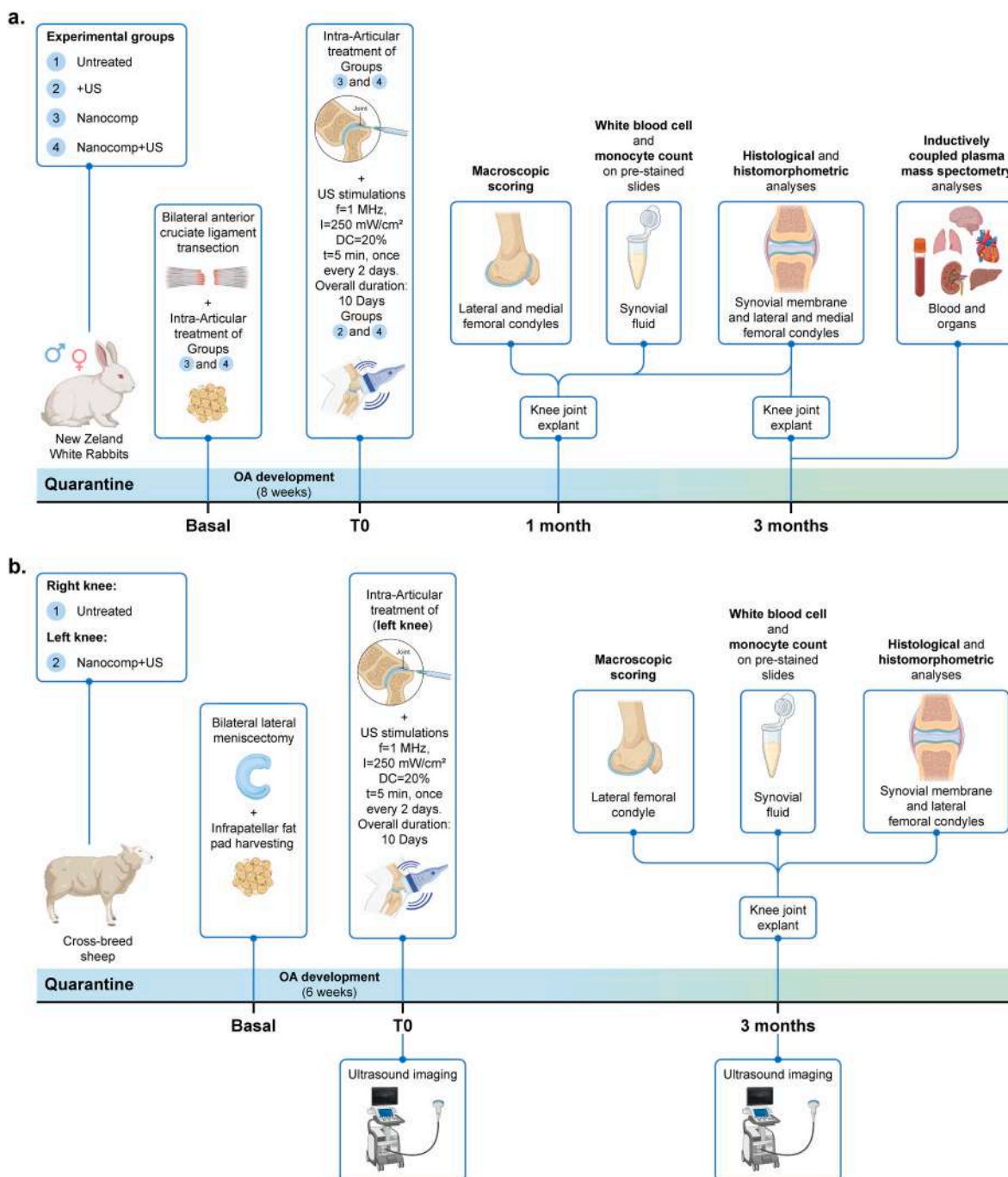


Fig. 2. Flow chart of the *in vivo* efficacy studies in (a) rabbit and (b) sheep OA models. T0 = starting point treatment after OA induction, f = frequency, I= Intensity, DC = duty cycle, t = exposure time.

constructive acoustic interference caused by the presence of two ultrasound beams. Thus, the transducer driving system's output voltage was set to achieve an intensity in the free field of 213 mW/cm² in the free field, which corresponded to an intensity of 250 mW/cm² at the target.

The effect of the knee flexion on the stimulation of the lateral condyle ROI was also studied. As expected, results summarized in Table S1 showed that knee flexion better exposed the condyles, thereby allowing for more effective stimulation (in terms of uniformity).

Following computational modeling, experiments were carried out following the workflow shown in Fig. 2.

2.2. Efficacy in vivo study on rabbits: cell characterization, histology and histomorphometry

Isolated ASCs from both male and female rabbits were characterized by flow cytometry for the expression of different markers. As shown in Fig. 3a, no differences were observed between sexes for any of the

markers analyzed. The ASCs were highly positive to CD29, CD44 and CD105 and negative to CD34 and CD45, confirming their previously reported phenotypic characteristics [33–36].

One hundred and four New Zealand SPF rabbits underwent bilateral anterior cruciate ligament transection (ACLT) surgeries (52 males and 52 females). Six animals (four male and two female) did not complete the protocol: two male and two female rabbits were lost for intra-operative and postoperative complications unrelated to the procedures, while two males were rehomed in authorized recovery facilities for animals used for scientific purposes (la Collina dei Conigli Onlus, Italy) due to insufficient ASC growth. Thus, a total of 98 animals (48 males and 50 females) were allocated to the four experimental groups: (1) untreated animals (Untreated), (2) animals treated only with LIPUS stimulation, but without nanocomposite injection (+US), (3) animals treated only with nanocomposite injection, but without LIPUS stimulation (Nanocomp), and (4) animals treated with both nanocomposite injection and LIPUS stimulation (Nanocomp +US). As signs of well-being and

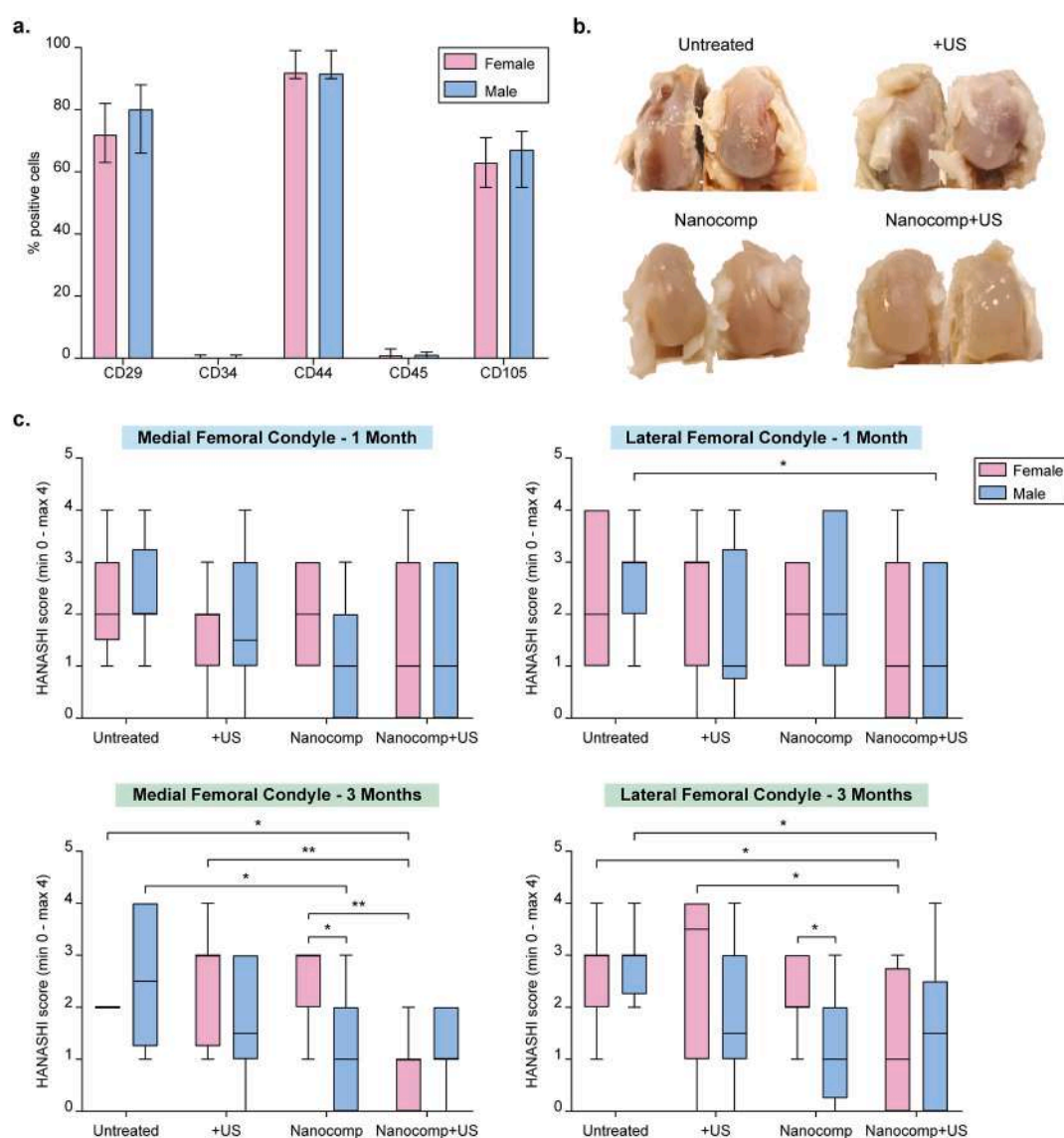


Fig. 3. ASCs characterization and macroscopic analyses on the rabbit OA model. (a) Flow cytometry analysis of CD29, CD34, CD44, CD45, CD105 on rabbit ASCs harvested from male and female animals; (b) Representative macroscopic images of medial and lateral femoral condyles explanted from female animals after 3 months; (c) Hanashi score results for medial and lateral femoral condyles of female (pink plots) and male (blue plots) rabbit joints after 1 and 3 months in the four groups: Untreated, +US, Nanocomp and Nanocomp +US. Generalized linear mixed models based on a Multinomial distribution followed by post hoc Sidak test were applied. Data are represented by box plots with median, 25th and 75th percentiles, minimum and maximum (n = 12). * $p < 0.05$; ** $p < 0.01$. (For interpretation of the references to color in this figure legend, the reader is referred to the Web version of this article.)

biocompatibility, body weight increased in all animals during the procedures, with no complications related to the treatments.

The Hanashi macroscopic score revealed significant improvements in cartilage surface and integrity at 3 months in female knees (Fig. 3b and c). Nanocomp +US female knees showed significantly better Hanashi score values compared to the other groups in the medial condyle, and to untreated and LIPUS-treated knees in the lateral compartment. In male rabbits, significant differences between Nanocomp +US and untreated animals were found at both 1 and 3 months only in the lateral femoral condyle. A trend (not statistically significant) toward a decrease in the Hanashi score was also observed for the medial femoral condyle. US and Nanocomp treatments appeared to yield superior outcomes in male compared to female cartilage across medial and lateral femoral condyles. However, statistically significant differences were observed at 3 months in the Nanocomp-treated male joints in comparison to female, and in the medial condyle versus Untreated.

Histological evaluation of the articular cartilage tissues at 1 month in the Untreated group revealed some diffuse signs of hypocellularity, cartilage discoloration and superficial fibrillation (Fig. 4 a) both in male and female animals. In contrast, Nanocomp +US-treated joints exhibited a more intense staining with Safranin O of the cartilage, indicating a higher proteoglycan content and reduced fissures or fibrillations (Fig. 4 a). The histological appearance was corroborated by the Safranin O staining measurements (Fig. 4 b): at 1 month, in the medial femoral condyle of female animal joints treated with Nanocomp +US, a significant lower Safranin O score was observed, compared to Untreated joints. Whereas the lateral condyle of female Nanocomp +US treated joints showed a significant lower Safranin O score than in all other treatment groups and compared to Nanocomp +US treated male. Moreover, female Untreated joints showed significantly worse scores than male ones. At 3 months, the effects of treatments showed less significant results: female Nanocomp +US-treated joints retained better Safranin O staining values than males, with significant improvements in comparison with +US and Nanocomp-treated joints at the medial compartment and versus Untreated joints at the lateral femoral condyles.

The development of OA was quantified by the OARSI score for both medial and lateral femoral condyles. As shown in Fig. 4 b, Nanocomp +US-treated female knees displayed significantly lower OARSI scores than the other groups, in both the medial and lateral compartments at 1 month, indicating a lower extent of OA. This result was not observed in male rabbits. Furthermore, significant differences in OARSI scores were noted between male and female animals in Nanocomp +US-treated joints after 1 month, for both the medial and lateral condyles.

When considering cartilage and bone histomorphometric parameters, such as Cartilage thickness (Ca.Th), Trabecular Separation (Tb.Sp) and Fibrillation index (FI), as shown in Figure S4 a, b, c, no significant differences were observed in Nanocomp +US group at both 1 and 3 months, for either male and female animals. Similarly, no significant differences were found in bone parameters, including subchondral bone plate thickness (Sbp.Th), trabecular thickness (Tb.Th), trabecular bone volume (Tb.BV) and trabecular number (Tb.N) in both the lateral and medial compartments (data not shown).

2.3. Efficacy in vivo study on rabbits: synovial fluid and membrane analysis

The inflammatory responses were evaluated by measuring the white blood cells (WBC) number in the joint synovial fluid. In general, the WBC count was significantly different between male and female animals across all experimental groups, both at 1 and 3 months. As shown in Fig. 5 a, after 1-month, female knees treated with LIPUS, or Nanocomp or Nanocomp +US, exhibited significantly higher WBC counts compared to untreated knees. Additionally, at both 1 and 3 months, female knees treated with Nanocomp and Nanocomp +US showed higher recruitment of WBC than male knees.

We also evaluated the presence of monocytes in the synovial fluids,

given their essential role in cartilage regeneration. Monocyte counts were performed after 1 month, when inflammation was more pronounced. The results (Fig. 5 b) clearly evidenced higher monocyte values in female animals compared to males. Specifically, female knees treated with Nanocomp and Nanocomp +US showed a significantly higher number of monocyte counts than their male counterparts.

The Krenn scores of the synovial membranes evidenced scores ranged from 2.1 to 4.6 points, corresponding to a low-grade synovitis, with no significant differences observed between the experimental groups or between the sexes (Fig. 5c and 5 d). Histopathological analyses showed thin synovial layers, with minimal signs of fibrosis or inflammatory infiltrates in all groups.

2.4. Biodistribution of Titanium and Barium in rabbit organs: Inductively Coupled-Plasma Mass Spectrometry analyses

To evaluate the potential distribution of Titanium and Barium ions from BNTPs in organs distant from the injection site, Barium (Ba) and Titanium (Ti) analytes were quantified by Inductively Coupled-Plasma Mass Spectrometry (ICP-MS) in blood and key organs of male and female rabbits treated and untreated with Nanocomp (Table 1). After 3 months, in Nanocomp-treated (+BaTiO₃) male and female rabbits, the concentrations of these analytes were comparable to those observed in untreated animals (-BaTiO₃), both in blood (the first distribution route), and in distant organs.

2.5. Sheep pilot study: cell characterization, histological and histomorphometric analyses

ASCs isolated from sheep confirmed a high percentage of cells positive to CD29, CD44, CD73 and CD105, and a low number of cells positive to CD34 and CD45 (Fig. 6 a), confirming their typical phenotypical characteristics as previously reported [37,38].

The macroscopic Hanashi score did not reveal significant differences between the Nanocomp +US and Untreated knees (Fig. 6b and c). However, histological images and the microscopic OARSI score, focusing on OA features of the articular cartilage, showed that the Nanocomp +US treatment had beneficial effects on the articular cartilage compared with untreated knees (Fig. 6d and e), confirming the results evidenced in the rabbit model. Histomorphometric analysis showed an increase in cartilage thickness in untreated joints compared to the treated ones (Fig. 6 f).

The Krenn score, which evaluates the grade of synovitis, showed no significant differences between the groups. (Figure S5 a,b). Cartilage smoothness and integrity, as assessed by the fibrillation index (FI), did not differ between treated and untreated knees (Figure S5 c). Finally, no significant differences were observed in Sbp.Th, Tb.Th, Tb.BV and trabecular separation (Tb.Sp) (data not shown).

In the sheep pilot study, we assessed the efficacy of the Nanocomp +US treatment in a large-sized animal model of KOA, comparing it to the untreated contralateral knee. This approach minimized intra-individual variability. The Nanocomp +US treatment showed improvement in OA signs at the microscopic level of articular surfaces, as evidenced by a reduction of the OARSI score. However, a decrease in cartilage thickness was observed (Fig. 6), although these values remained within the typical range of femoral articular cartilage of sheep [39,40].

2.6. Sheep pilot study: ultrasonography and synovial fluid and membrane analysis

In Figure S5 d, ultrasound images of left and right ovine knees before (T0) and after treatments (3 months) are shown. After meniscectomy, reduced thickness of femoral condyle articular surfaces and peritendinous synovial fluid effusion (indicative of tenosynovitis) were observed. At the 3-month endpoint, articular cartilage appeared thinned in both treated and untreated knees. However, synovial fluid reabsorbed

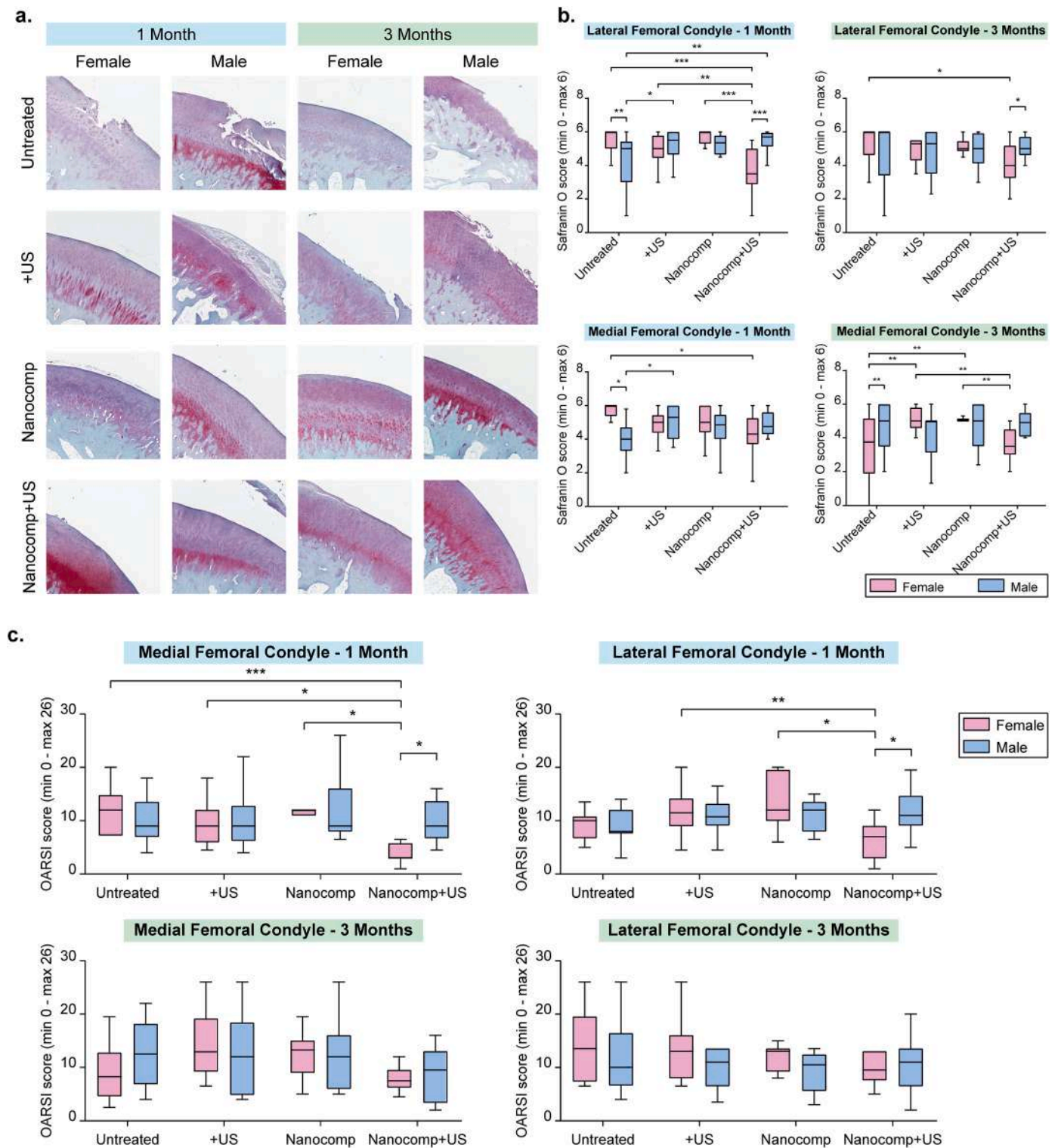


Fig. 4. Histological and microscopic analyses of femoral condyles on the rabbit OA model. (a) Representative histological images of the articular cartilage (lateral femoral condyles) of female and male rabbits at 1 month and 3 months. Safranin O/Fast green staining, 10x magnification (bar = 300 μm); (b) Safranin O staining score results of medial and lateral femoral condyles of female (pink box plot and whiskers) and male (blue box plot and whiskers) rabbit joints after 1 and 3 months in the four groups: Untreated, +US, Nanocomp and Nanocomp +US. Generalized linear mixed models based on lognormal distribution with post hoc Sidak test were applied. Data are represented by box plots with median, 25th and 75th percentiles, minimum and maximum (n = 12). *p < 0.05, **p < 0.01; ***p < 0.001. (c) Microscopic OARSI score results of medial and lateral femoral condyles of female (pink box plot and whiskers) and male (blue box plot and whiskers) rabbit joints after 1 and 3 months in the four groups: Untreated, +US, Nanocomp and Nanocomp +US. Generalized linear mixed models based on Gamma distribution with post hoc Sidak test were applied. Data are represented by box plots with median, 25th and 75th percentiles, minimum and maximum (n = 12). *p < 0.05, **p < 0.01; ***p < 0.001. (For interpretation of the references to color in this figure legend, the reader is referred to the Web version of this article.)

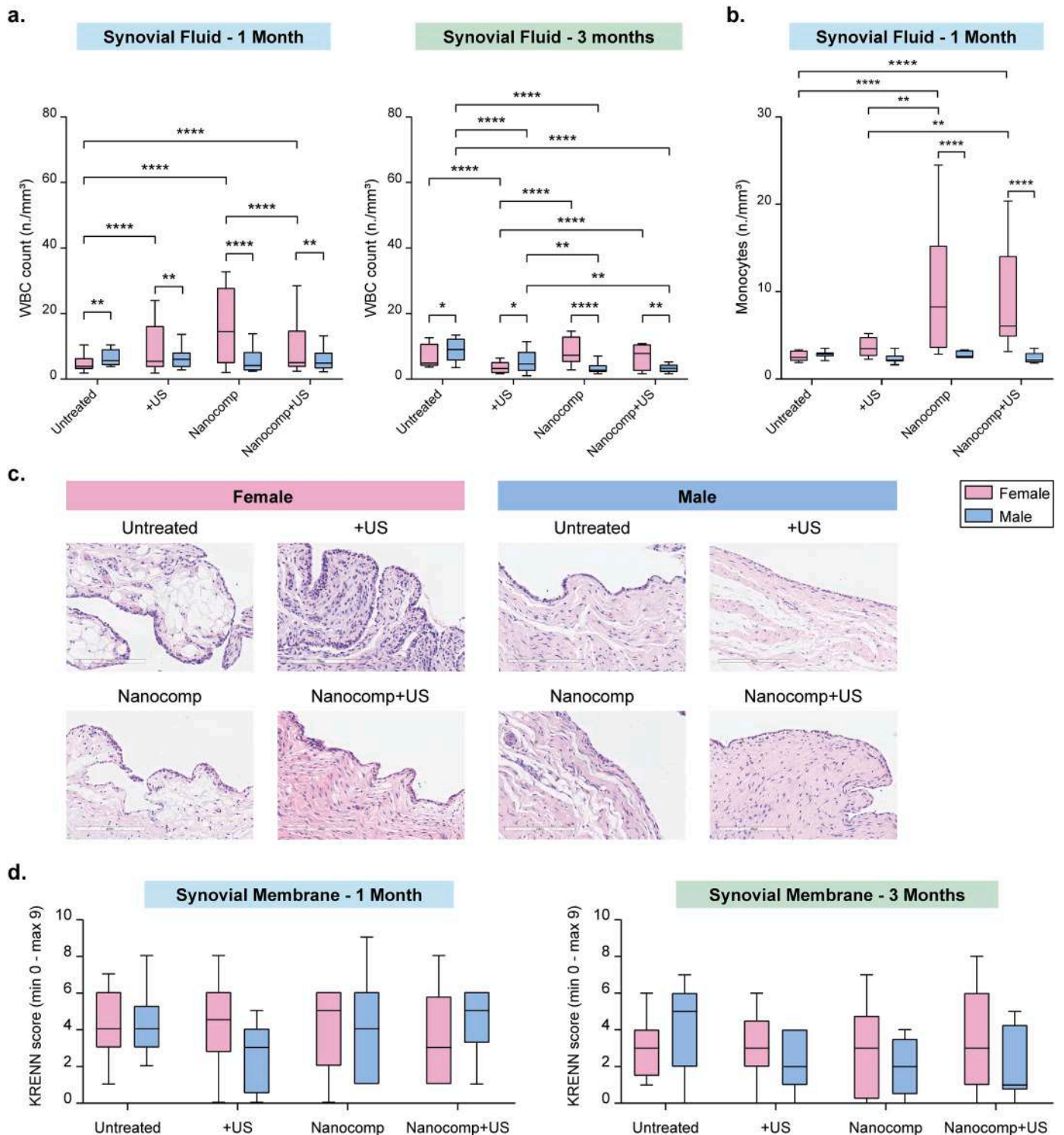


Fig. 5. Inflammatory responses and synovial membrane histopathological results. (a) WBC count in synovial fluid of female (pink plots) and male (blue plots) rabbits after 1 and 3 months; Generalized linear mixed models based on Poisson distribution with post hoc Sidak test (b) Monocyte cell count in synovial fluid of female (pink plots) and male (blue plots) rabbits at 1 month. Generalized linear mixed models based on Tweedie distribution with post hoc Sidak test were applied. Data are represented by box plots with median, 25th and 75th percentiles, minimum and maximum (n = 10). **p* < 0.05; ***p* < 0.01; *****p* < 0,0001 (c) Representative histological images of the synovial membrane of male and female rabbits at 1 month, in the four groups: Untreated, +US, Nanocomp, Nanocomp +US. Haematoxylin-Eosin staining, 20x magnification, bar = 200 μm; (d) Krenn score results of synovial membranes of female (pink plots) and male (blue plots) rabbits after 1 and 3 months. Generalized linear mixed models based on Gamma distribution with post hoc Sidak test for pairwise comparisons, were applied. Data are represented by box plots with median, 25th and 75th percentiles, minimum and maximum (n = 12). (For interpretation of the references to color in this figure legend, the reader is referred to the Web version of this article.)

Table 1

Concentrations of Titanium (Ti) and Barium (Ba) analytes measured through ICP-MS, in animals' blood and main organs.

Tissue	Analyte	Male rabbits			Female rabbits		
		- BaTiO ₃ mg/kg	+ BaTiO ₃ mg/kg	<i>p</i> value	- BaTiO ₃ mg/kg	+ BaTiO ₃ mg/kg	<i>p</i> value
Blood	Ti	0,003 (0,001)	0,004 (0,001)	0,567	0,003 (0,000)	0,003 (0,001)	0,624
	Ba	0,011 (0,018)	0,021 (0,024)	0,327	0,017 (0,029)	0,022 (0,030)	0,683
Liver	Ti	0,036 (0,002)	0,042 (0,009)	0,310	0,054 (0,007)	0,044 (0,015)	0,246
	Ba	0,028 (0,005)	0,006 (0,000)	0,002	0,005 (0,005)	0,001 (0,007)	0,263
Heart	Ti	0,017 (0,003)	0,013(0,006)	0,350	0,016 (0,006)	0,014 (0,007)	0,786
	Ba	0,029 (0,002)	0,028 (0,034)	0,558	0,028 (0,045)	0,008 (0,012)	0,310
Kidney	Ti	0,069 (0,006)	0,038 (0,001)	0,001	0,064 (0,017)	0,061 (0,018)	0,779
	Ba	0,027 (0,003)	0,062 (0,044)	0,243	0,002 (0,011)	0,002 (0,007)	0,310
Lung	Ti	0,015 (0,005)	0,011 (0,003)	0,279	0,011 (0,008)	0,010 (0,003)	0,731
	Ba	0,028 (0,010)	0,023 (0,024)	0,754	0,000 (0,011)	0,007 (0,017)	0,557
Brain	Ti	0,023 (0,002)	0,018 (0,008)	0,357	0,030 (0,011)	0,034 (0,012)	0,623
	Ba	0,038 (0,001)	0,039 (0,026)	0,933	0,042 (0,018)	0,037 (0,026)	0,781

Ti and Ba concentrations were measured in the blood and the main organs of male and female rabbits that received an intraarticular injection of Nanocomp (+BaTiO₃) or were untreated (-BaTiO₃) after 3 months. Analyte concentrations are expressed as mean (standard deviation). The *p* value has been obtained by comparing + BaTiO₃ and - BaTiO₃ values with a Student's *t*-test, for each group.

within the tendon sheath in the Nanocomp +US-treated knee, resulting in less tenosynovitis compared to the Untreated knee.

Similar to the rabbit efficacy study, we quantified the levels of the main inflammatory cytokines (IL-1 β , IL-6, IL-8 and TNF α), as well as WBC and monocytes in the synovial fluid to assess the local inflammatory status. No significant differences in WBC and monocyte counts were observed between Untreated and Nanocomp +US treated knees (Figure S6 a, b). Furthermore, the levels of inflammatory cytokines (Fig. S6c–f) showed no significant differences between the two groups.

3. Discussion

To the best of our knowledge, no prior studies have precisely delivered an ultrasound dose to the target tissue, carefully considering the complex anatomy of animal joints and the corresponding acoustic phenomena such as reflections, attenuations and standing wave formations. The results shown in Fig. 1, S1, S2, S3 represent a significant methodological innovation in the field of LIPUS stimulation. Our approach predicts the optimal settings to ensure the delivery of the desired amount of mechanical energy to the target tissue, thus maximizing the reliability of *in vivo* experimental outcomes. These methodologies allow for calibrated LIPUS stimulation by considering the anatomical features of each animal model. Our *ad hoc* simulations predict the propagation of the acoustic beam until it reaches the target, in this case, the cartilage tissue on femoral condyles.

In addition to computational models for predicting *in vivo* LIPUS stimulation, another significant scientific advancement in this study involves the investigation of sex-related therapeutic effects. It is well-established that cartilage degeneration and regeneration in humans are sex-dependent [41], influenced by hormones and specific features of OA progression [42]. Women exhibit a higher prevalence of cartilage damage due to traumas or pathologies compared to men [43]. In our study, we assessed the impact of the proposed treatment in the rabbit OA model, considering animal sex, an aspect that is often overlooked in *in vivo* studies [44–48]. The experimental time-points were selected based on the degradation timeline of the Nanocomp, which has been evaluated to be resorbed within 3 months [22]. Our findings indicate that the combination of the piezoelectric 3D nanocomposite enriched with autologous ASCs and stimulated with LIPUS significantly slowed the progression KOA both at the macroscopic and microscopic levels. The macroscopic evaluations of the cartilage characteristics, at both 1 and 3 months, revealed that Nanocomp treated with LIPUS significantly counteracted the development of OA (Fig. 4 c). Interestingly, differently from macroscopic results, no differences were observed in

histomorphometric parameters related to bone architecture. This could be due to the use of a semi-quantitative macroscopic score [49], widely used to assess the gross morphology of articular cartilage. Indeed, such a score is based on a four-point scale considering surface smoothness, colour, and the presence of erosion or fibrillation, and cannot consider the deeper layers of articular cartilage and the subchondral bone. We used the OARSI score and histomorphometric features to evaluate OA progression, using high-resolution images acquired by a digital pathology scanner and analyzed through a high-throughput software. The absence of significant changes in bone-related histomorphometric parameters suggested that the subchondral compartment was not affected by OA. This was also consistent with the selected surgical model of OA induction, which typically leads to a mild form of post-traumatic OA. In fact, the histological features of the rabbit OA model usually include loss of Safranin O staining, cartilage fissures and erosion, chondrocyte depletion and clustering, while the tidemark remained preserved [50, 51]. However, the positive effects of the treatment on both the medial and lateral condyles were more pronounced in female animals than in male, emphasizing the impact of sex on treatment efficacy. Notably, the treatment's effectiveness was more apparent at the 1-month time point, with some persistence observed at 3 months, but primarily in the femoral lateral condyle of female animals. These findings are corroborated by previous *in vitro* [22] and *in vivo* [52] results. *In vitro*, it was shown that ASCs, in Nanocomp +US, retained viability and chondrogenic commitment up to 28 days [22]; *in vivo*, using the same rabbit OA model, it was found that labelled ASCs survived 1 month in the knee joint, exhibiting a preferential migration toward injured areas of articular cartilage compared to other joint tissues (i.e., synovia, meniscus, ligaments, and synovial fluids) [52]. The long-term survival of ASCs at 3 months was not investigated; in the literature, the use of fluorescence cell dyes has been reported to have limited *in vivo* duration (up to 70 days) [53,54]. Moreover, it has been shown that ASCs have multifaceted therapeutic efficacy, not only strictly dependent on their potential to differentiate into chondrocytes, but also related to paracrine factors (i.e., soluble factors, extracellular vesicles, secretome) able to maintain chondrocyte homeostasis, counteract inflammation and reduce the catabolic OA microenvironment [55,56]. Therefore, the observed decrease in efficacy at 3 months suggests that repeated treatments may be necessary to achieve long-term positive effects (Fig. 5 b).

In addition, sex differences might be related to the varying potency of isolated autologous ASCs in terms of secretion of trophic and paracrine growth factors. In fact, human ASCs have shown sex-based differences in hormone profiles and transcriptome, which could ultimately affect tissue repair properties [57–61].

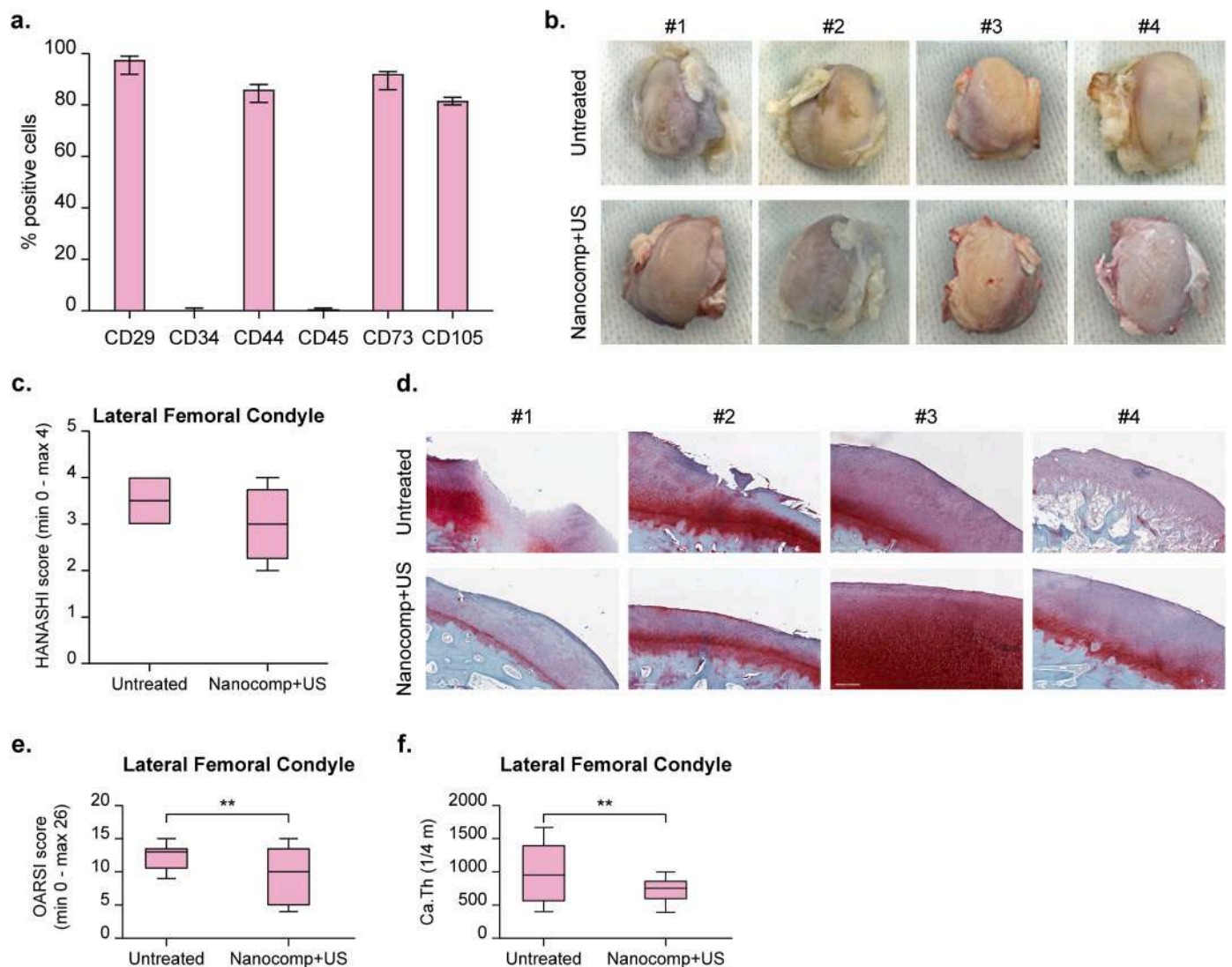


Fig. 6. ASCs characterization, macroscopic and histomorphometric analyses on sheep OA model. (a) Flow cytometry analysis of sheep ASCs for positive (CD29, CD 44, CD73, CD105) and negative (CD34, CD45) markers; (b) Macroscopic images of all explanted Untreated and Nanocomp +US treated lateral femoral condyles (#1, #2, #3, #4) at 3 months; (c) Hanashi score of Untreated and Nanocomp +US treated joints after 3 months. Wilcoxon test followed by Monte Carlo is applied. Data are represented by box plots with median, 25th and 75th percentiles, minimum and maximum; (d) Histological images of the articular cartilage of lateral femoral condyles at 3 months. Safranin O/Fast green staining, 10x magnification (bar = 300 μ m); (e) Microscopic OARSI score of Untreated and Nanocomp +US treated joints after 3 months. General linear model based on Gamma distribution was applied. Data are represented by box plots with median, 25th and 75th percentiles, minimum and maximum. **p < 0.01; (f) Cartilage thickness of Untreated and Nanocomp +US treated joints after 3 months. Generalized linear model with Gamma distribution was applied; data are represented by box plots with median, 25th and 75th percentiles, minimum and maximum. **p < 0.01. (For interpretation of the references to color in this figure legend, the reader is referred to the Web version of this article.)

Interestingly, our study is the first to evaluate the therapeutic efficacy of a multi-approach treatment (ASCs, nanocomposite hydrogels, and LIPUS) in animal models of OA, accounting for sex differences. A recent systematic review highlighted the lack of preclinical *in vivo* studies exploring OA treatment in experimental rabbit model of both sexes [62]. While Liu and Vinikoor investigated piezoelectric materials for cartilage regenerative in rabbits, they did not consider sex differences and employed a critical-sized osteochondral defect model, rather than an OA model [63,64]. Moreover, there are no large randomized clinical trials directly comparing the effectiveness of treatments for OA, according to sex as the primary endpoint. Based on our findings, we suggest that repeated intra-articular injections may be needed to achieve a long-lasting effect, especially in male animals. Moreover, the reduced efficacy observed in males indicates the need for more frequent intra-articular applications or higher cell densities. These results underscore the importance of considering sex as biological variable from bench to

bedside.

Chronic inflammation is a hallmark of OA, driving cartilage degradation and bone remodelling. This cycle is perpetuated by the secretion of inflammatory cytokines, which further exacerbate cartilage destruction [65,66]. To our knowledge, no preclinical ACLT studies in both sexes exist to directly compare WBC/monocyte recruitment patterns. Although, it was not an objective of our study, we found that the synovial fluid of female rabbits had significantly higher numbers of WBC and monocytes than that of male animals after 1 month. Notably, these increases in WBC and monocytes were correlated with improvement in the microscopic evaluation of OA patterns, as indicated by the OARSI score (Fig. 4). We speculate that the immunomodulatory effects in females on WBC and monocyte may be attributed primarily to the presence of Nanocomp (\pm US) and confined to inflammatory characteristics of OA. In contrast, at the histological level, the therapeutic efficacy seems to result from the combined action of Nanocomp +US, which acts

synergistically to slow down the progression of OA. BTNPs nanoparticles contained in the Nanocomp hydrogel are supposed to possess immunomodulatory properties, capable of mobilizing and recruiting macrophages while acting as nanogenerators under LIPUS stimulation. Piezoelectric nanoparticles, in fact, can generate electric fields under mechanical stimulation, potentially guiding macrophages towards a pro-regenerative M2 phenotype. This hypothesis is supported by previous studies showing that organic, inorganic or hybrid nanoparticles were able to promote M2 differentiation, enhancing tissue regeneration and reducing pro-inflammatory M1 population [67–71]. In particular, Wu et al. showed that the M1/M2 switch in BaTiO₃ scaffolds is mediated by the up-regulation of PI3K/Akt phosphorylation and the down-regulation of Notch signaling pathways [72–74], suggesting that the confirmation of this hypothesis would be the focus of future studies.

The evaluation of nanomaterial-based medical devices, particularly for safety and biocompatibility, remains underdeveloped. The technical note ISO/TR10993-part 22 (2017) gives guidance on nanomaterials, but no specific standardized procedures guide researchers toward a comprehensive assessment. Titanium is known to persist in tissues and cells [75,76]; in our previous work [22], we found that BNTPs could be internalized in cell vacuoles within the cytoplasmic membrane, *in vitro*. In this study, we assessed the potential toxicity of BNTPs in the hydrogel by measuring Titanium and Barium ions in the blood and organs distant from the injection site to exclude any accumulation that could have raised safety issues. We found no evidence of accumulation in distant organs, suggesting that the nanomaterials did not pose any bioaccumulation risks. These findings represent an important advancement, as the bioaccumulation of nanomaterials and their fate is often unexplored in the literature [77].

Several preclinical *in vivo* studies have demonstrated, in animal models of knee OA, that the articular cartilage may appear thicker in the early stages due to cartilage swelling and chondrocyte hypertrophy. This phenomenon cannot be attributed to an ongoing tissue repair, but rather to damage. In clinical studies, involving cohorts of knee OA patients, a high degree of variability in cartilage thickening and degeneration is observed among OA patients [78–81].

However, no similar studies are available in sheep models. Vahedi and colleagues [82] investigated the regenerative effects of LIPUS on surgically induced cartilage defects, while Feng and colleagues [83] combined hyaluronic acid with autologous and allogenic ASCs to prevent OA progression in a different surgical model [84]. Veronesi et al. [85] used the same OA animal model to compare the efficacy of allogenic amniotic epithelial stromal cells and ASCs in slowing down the disease evolution, but without a biophysical stimulation.

The major limitation of this pilot sheep study is the small sample size, which might affect the statistical significance of results. Furthermore, the pilot study on the sheep reflected a chronic disease, as evidenced by the absence of differences in inflammatory cytokines and WBCs counts, which instead are typically observed during the early acute phase [86–88], as we evidenced in rabbits at one month. On the other hand, this model provides significant translation relevance, as it closely mirrors humans' joint dimensions, structure, anatomy and cartilage composition. The developed computational model also ensures the applicability of the LIPUS device and setting, guaranteeing the reliability and uniformity of stimulation to the target area. Indeed, this study is a critical step towards evaluating the efficacy of this personalized treatment for early-stage OA in large animal model before clinical translation.

In both preclinical models, we adopted a standardized surgically induced OA model: anterior cruciate ligament transaction in rabbits and lateral meniscectomy in sheep, both of which cause a mild-to-moderate OA [50,85,89–93]. This OA grade was confirmed by our histomorphometric evaluations, in which subchondral and epiphyseal trabecular bone remained unaffected.

From a translational point of view, the resolution of the early OA grades is highly relevant, and it would enable patients to return to

normal daily life activities and delay the need for more invasive treatments.

4. Conclusion

In conclusion, we demonstrated that a nanocomposite hydrogel embedding adipose-derived stromal cells and stimulated with a calibrated dose of low-intensity pulsed ultrasound, selected through computational models that considered the animal joint anatomy, was effective in slowing down both the macroscopic and microscopic hallmarks of knee osteoarthritis progression in medium- and large-sized animal models. Moreover, our results highlighted the importance of considering sex in preclinical studies, which better mirror the clinical situation, where sex significantly impacts the onset, progression and therapeutic treatments of osteoarthritis. Future studies could investigate whether cartilage regeneration induced by the nanocomposite hydrogel stimulated with US is driven by transplanted ASCs, endogenous cartilage progenitors, or a combination of both factors.

5. Experimental methods

5.1. Computational models for *in vivo* ultrasound stimulation

The development of the computational models involved the following phases: (1) the creation of the 3D model of the animal from anatomical images (either CT or MR) by segmenting the most relevant tissues from an acoustic point of view (i.e., skin, muscle, fat, bone, tendons and ligament); (2) the definition of the ROIs corresponding to the condyle regions where cartilage lesions are most likely to occur (3) the interactive positioning of the transducer(s) with respect to the reconstructed model; (4) the development of acoustic simulation using the k-Wave solver [94] on the virtual set-up developed; (5) the visualization of the 3D pressure maps directly on the animal model anatomy and/or anatomical images, as well as record the pressure distribution on the ROIs.

Anatomical images were segmented using 3D Slicer [95] segmentation tools and to each segmented tissue, specific acoustic properties were associated. Once the virtual set-up was defined, the scenario was translated into a format compatible with the k-Wave solver. The same simulation parameters were used for both rabbits and sheep. The acoustic source was modeled as a disc representing a mono-element piston-shaped transducer having a diameter of 23 mm and working at a frequency $f = 1$ MHz. Taking into account animal anatomy, for the rabbit, the transducer was positioned parallel to the skin (at, approximately, 45° with respect to the tibial plateau), whereas, for the sheep, two transducers (with the same characteristics) were used to cover the whole joint space. For improving acoustic coupling, stand-off gel pads (Aquaflex, Parker Laboratories, Fairfield, NJ, USA) were placed between the transducer and the animal skin. This set the transducer-to-skin distance at 2 cm (i.e. the thickness of the gel pad).

The tissue acoustic parameters were retrieved from the IT'IS online database (IT'IS Database for thermal and electromagnetic parameters of biological tissues, Version 4.1, Feb 22, 2022, DOI: 10.13099/VIP21000-04-1. itis.swiss/database) [96]. The nanocomposite hydrogel was not included in the simulations, as it can be considered acoustically transparent, given that its acoustic properties are comparable to those of soft tissues and are not significantly altered by the presence of nanoparticles at the tested concentrations, as previously demonstrated [97].

For each model, a ROI within the condyle area was defined to include the region more subjected to cartilage lesions. After running acoustic simulations, a pressure distribution analysis was carried out over these ROIs to evaluate attenuation and stimulation uniformity (which has been shown to be a critical parameter for effective chondrogenesis *in vitro* [22]). A uniformity score was then defined as the percentage of voxels stimulated at the target intensity (i.e., 250 mW/cm²) with a tolerance of ±30 %.

Finally, the attenuation factor due to the presence of the gel pad and tissue interfaces was calculated as the ratio between the median value of the simulated pressure within the animal model condyle ROI and the median value of the simulated pressure distribution theoretically acting on the hydrogel sample in the *in vitro* set-up. Such a value was then used in the *in vivo* experiments to set the ultrasound generator gain, thus obtaining *in situ* intensity values comparable to those the samples were exposed to *in vitro*.

5.2. Ethics and legal requirements

In vivo studies were performed by following the Italian Law by Decree 26/2014 on the protection of animals used for scientific purposes and according to the European Commission Recommendation on guidelines for the accommodation and care of animals used for experimental and other scientific purposes (2007/526/EC). The protocols were developed in accordance with the Planning Research and Experimental Procedures on Animals: Recommendations for Excellence – PREPARE - [98] guidelines and the research reports were set according to the criteria defined in the Animal in Research: Reporting in Vivo Experiments-ARRIVE - guidelines [99].

The *in vivo* experiments on the rabbit model were firstly approved by the Animal Welfare Body of the IRCCS Istituto Ortopedico Rizzoli (IOR) and then authorized by the Italian Ministry of Health (Authorization N. 418/2022-PR). To monitor animal wellbeing and welfare, animals were weighed and clinically evaluated daily in the first week and then weekly after surgery. The following humane endpoints were considered to avoid animal suffering: loss of body weight greater than 20 % of their physiological growth curve, severe limb lesions or irreversible alterations in general or primary organic functions, severe pain non-treatable pharmacologically. Criteria that determined the exclusion from analyses were severe intra-anaesthesiologic complications, knee infections, or humane endpoint achievement.

The *in vivo* experiments on the sheep model were firstly approved by the Animal Welfare Body of the IOR and then authorized by the Italian Ministry of Health (Authorization N. 746/2023-PR). A clinical evaluation of the animals was performed daily in the first week and then weekly, and any symptoms or distress were monitored by a specific pain score and Grimace scale [100]. The following humane endpoints were *a priori* defined: loss of body weight greater than 20 % of their physiological growth curve, prolonged (more than 72 h) decubitus, severe limb lesions or irreversible alterations in general or major organic functions, severe pain non-treatable pharmacologically, pain score >10 points. The criteria for excluding animals from the analyses were severe intra-anaesthesiological complications, knee infections, or humane endpoint achievement.

5.3. Isolation and characterization of rabbit and sheep stromal cells

Autologous rabbit infrascapular adipose tissue (2.9 ± 1.0 gr.) and autologous sheep infrapatellar fat pad (5.6 ± 1.0 gr.) were surgically removed under general anesthesia and weighted, then washed in Dulbecco's Phosphate-Buffered Saline (D-PBS, Aurogene Srl, Italy) and enzymatically digested in a 0.075 % collagenase type II (Gibco, USA) solution at 37 °C with continuous agitation for 2 h for ASCs isolation. The enzymatic reaction was stopped by adding Dulbecco's Modified Eagle Medium (DMEM) low glucose with 10 % fetal bovine serum (FBS, Euroclone, Italy) and the solution was centrifuged at $300 \times g$ for 5 min. After several D-PBS washing steps, the ASCs pellet was resuspended, counted and $50,000$ – $100,000$ cells/cm² were seeded in a T25 flask. Cells were cultured and expanded in sterile and standard conditions (37 °C, 5 % CO₂) and the culture medium was changed twice a week up to cell passage 2. The isolated cells were evaluated for the expression of different markers by flow cytometry. The immunophenotype of rabbit and sheep ASCs was analyzed using a BD FACS Canto II flow cytometer (Becton Dickinson, New Jersey, US). Markers were analyzed using anti-

CD29 fluorescein isothiocyanate (FITC) (Becton Dickinson), anti-CD34 phycoerythrin (PE) (Gene Tex, Maryland, US), anti-CD44 PE (Novus, Missouri), anti-CD45 FITC (Gene Tex), and anti-CD105 FITC (GeneTex). The samples were diluted and incubated in PBS supplemented with 0.2 % sodium azide (NaN₃) (Sigma-Aldrich, Missouri, US) and 2 % FBS for 30 min at 4 °C. Samples were then washed with PBS and analyzed with the above-mentioned flow cytometer.

5.4. Preparation of the injectable nanocomposite hydrogel

Nanocomposite hydrogel preparation was performed as previously reported [22]. Briefly, the VitroGel-RGD® solution (The Well Bioscience, North Brunswick, NJ, USA) was mixed with the Dilution Solution Type 1® (The Well Bioscience) at the ratio 1:2 up to obtain a uniform mixture. GO nanoflakes and BTNPs were added at 25 µg/mL and 50 µg/mL, respectively. Then, DMEM (Life Technologies, Bleiswijk, The Netherlands) with a suspension of rabbit or sheep ASCs to reach the final cell density into the hydrogel of 2×10^6 cells/mL was added at the ratio of 4:1 (pre-crosslinked solution: DMEM with cells) and mixed in a syringe with a 22G needle.

5.5. *In vivo* efficacy rabbit model: experimental study design and surgical procedures

One hundred and four adults CrI:KBL New Zealand (NZW) Specific Pathogen Free rabbits of both sexes (Charles River Laboratories, mean weight male 2.4 ± 0.2 kg, female 2.5 ± 0.2 kg) specifically bred for life science studies were used. The animals were received from the vendor of the same age and housed in the same stabling conditions. No randomization was applied to allocate animals to groups; outcome assessors were blind to the allocation groups.

The animals were housed in single cages in standard controlled conditions with free access to water and pellet diet and specific enrichments. Surgical procedures were performed after a 10-day quarantine period under general anesthesia induced by intra-muscular injections of ketamine (44 mg/kg, Imalgene 1000, Italy) and xylazine (0.3 mg/kg, Rompun 25 ml, Bayer S.p.A., Italy) and maintained by spontaneous breathing with O₂/air and isoflurane 2–3 % with a facial mask. Male and female rabbits underwent bilateral ACLT for OA induction [89]: a 2 cm skin and capsular incision was carried out in a lateral approach; the patellar bone was displayed laterally with the knee placed in full flexion, anterior cruciate ligaments (ACLs) were exposed and transected. Then, the articular capsule and skin layers were sutured. Within the same surgical session, in groups treated with Nanocomp., the infrascapular adipose tissue was surgically dissected for ASCs isolation and expansion. In the immediate post operative period and for 5 days, analgesic (50 mg/kg die, Farnolisina, Italy, 17 µg/72 h fentanyl transdermal patch, FenPatch, Ratiopharm, Germany and 3.75 mg of a solution 7.5 mg/ml of Ropivacaina S.A.L.F, Italy) and antibiotic (10 mg/kg enrofloxacin, Baytril, Elanco Italia S.p.A.) therapies were administered.

Eight weeks after OA induction (T0), animals were allocated into four groups: (1) Untreated, (2) + US, (3) Nanocomp, (4) Nanocomp +US. Rabbits from the Nanocomp and Nanocomp + US groups received 0.3 mL bilateral i.a. injections of ASCs-laden Nanocomp. Rabbits from the +US and Nanocomp +US groups were locally treated with LIPUS (frequency: 1 MHz, intensity = 250 mW/cm², duty cycle = 20 %, exposure time: 5 min every 2 days, for an overall duration of 10 days), as carried out during *in vitro* experiments. Based on computational models, a LIPUS transducer was applied frontally to each joint in full flexion by using a gel pad (Aquaflex Ultrasound Gel Pad, Parker Labs, USA).

At the selected experimental time-points (1 and 3 months), rabbits were pharmacologically euthanized under deep general anesthesia with intravenous administration of 1 mL of Tanax® (Hoechst AG, Frankfurt-am-Main, Germany). Blood, main organs (brain, heart, lung, liver and kidney), synovial fluids, synovial membranes and femoral condyles were harvested and processed for the analyses, as described in the following

sections. The experiment workflow is depicted in Fig. 6 a.

5.6. *In vivo sheep pilot study: experimental study design and surgical procedures*

Four adult cross-breed sheep were used (mean weight 47.1 ± 6.8 kg, IZS Marche ed Abruzzo “G.Caporale”, Teramo, Italy), housed in single boxes and fed with a standard pellet diet, hay and water *ad libitum*.

After quarantine, general anesthesia was induced with an intramuscular injection of 10 mg/kg ketamine and 0.3 mg/kg xylazine and a subcutaneous injection of 0.0125 mg/kg atropine sulphate. Then, general anesthesia was maintained by an intravenous injection of sodium thiopental in a 2.5 % solution and 2–3 % isoflurane administration (IsoFlo, Zoetis, Italy), in O₂/air 60 %/40 %, 7.5 l/min (Servo Ventilator, 900D; Siemens, Germany). For OA induction, bilateral lateral meniscectomy was performed [101]. For ASCs isolation, the infrapatellar fat pad (Hoffa’s fat pad) was surgically removed [102]. Skin and articular capsule incisions were made through a lateral paratrotuleal access; the synovial fluid was harvested, and the Hoffa’s fat pad carefully dissected for ASCs isolation and *in vitro* expansion. Then, the cranial and lateral attachments of the lateral meniscus were transected, removing entirely the meniscus. Analgesic and antibiotic therapies were administered, as described for rabbits, with free movements and fully weight bearing allowed.

Six weeks after surgery, left knees received a 1 mL intra-articular injection of the Nanocomp, followed by LIPUS stimulation (frequency = 1 MHz, intensity = 250 mW/cm², duty cycle = 20 %, exposure time: 5 min every 2 days, for an overall duration of 10 days). Two LIPUS transducers were applied, one medially and one laterally to the joint kept in a 15-degree flexed position, by applying gel pads (Aquaflex Ultrasound Gel Pad, Parker Labs, USA). Contralateral right knees were left untreated, serving as controls that spontaneously developed OA. Three months after starting the treatments, the animals were pharmacologically euthanized by intravenous injection of Tanax® (Hoechst AG, Frankfurt-am-Main, Germany). Synovial fluid and synovial membrane, as well as lateral femoral condyles of both joints, were harvested for analysis.

5.7. *Histological and histomorphometric analyses*

Explanted condyles from rabbit and sheep knee joints and synovial membranes were fixed in 4 % neutral buffered formalin solution for at least 48 h; bone specimens were decalcified in formic and hydrochloric acids solution and dehydrated, cleared in xylene and embedded in paraffin. A rotary microtome (Microm HM355 S, Thermo Scientific) was used to cut 5 ± 1 μm thickness sections. Femoral condyle slices were stained with 1.5 % Safranin-O solution (Polysciences, USA) and 0.02 % Fast Green (Polysciences, USA), whereas synovial membranes were stained with Haematoxylin/Eosin (BioOptica, Italy). All stained slices were digitalized through an Aperio Scanscope Digital Scanner (AT2, Leica BioSystems) at maximum magnification (40X).

Gross evaluation of lateral and medial femoral condyles from rabbit and lateral condyles from sheep knee joints was performed through a macroscopic assessment. According to the OARSI histopathology initiative [50], the semiquantitative Hanashi scoring system [49] was applied to evaluate the gross morphology and appearance of condyles: 0 - surface smooth with standard color; 1 - surface rough with minimal fibrillation or a slight yellowish discoloration; 2 - cartilage erosion extending into the superficial or middle layers; 3 - cartilage erosion extending into deep layers; 4 - complete cartilage erosion with subchondral bone exposure.

Synovial tissue was assessed by Krenn score for synovitis features [103] by semiquantitative evaluating the enlargement of the synovial layer, the density of the resident cells, and cellular phenotypes of the inflammatory infiltrate. Femoral condyles were assessed for OA by applying the OARSI semiquantitative score, which is the product of OA

grade (severity) and stage (extent). It ranges from a maximum score of 26 points (worst OA scenario) to a minimum of 0 points (healthy cartilage) [104]. Safranin O staining was evaluated by applying a modified validated scoring system for detecting articular cartilage changes in the ACLT rabbit model [50]: it ranges from a maximum score of 6 (loss of staining in all the four zones of articular cartilage ≥ 50 % the length of the condyle) to a minimum of 0 points (uniform staining throughout articular cartilage).

Moreover, prominent histomorphometric bone and cartilage parameters such as cartilage surface FI, Ca.Th, Sbp.Th and the bone microarchitecture, assessed through Tb.Sp, Tb.N, Tb.Th, trabecular bone surface and Tb.BV, were quantitatively evaluated using the Bioquant Osteo software (Bioquant Osteo 2022 Version 22.5.60 ME, BIOQUANT Image Analysis Corporation). All the bone-related parameters were evaluated in a ROI spanning from the maximal loading zone up to 2 mm in depth. Sbp.Th was evaluated as the mean of the transversal thickness measurement conducted throughout the subchondral plate every 200 μm. Similarly, a ROI comprising the above cartilage was selected and Ca.Th measurement was considered. Concerning FI measurement, the original cartilage ROI was subdivided into four smaller ROIs to limit the effect of tissue curvature. Thus, FI was carried out on each micro-ROI by dividing the cartilage perimeter length by the length of the micro-ROI.

5.8. *Echographic evaluations*

Ultrasound analysis of both sheep joints was performed through an ArtUs EXT Digital Ultrasound Diagnostic System (TeleMed Ultrasound Medical Systems, Vilnius, Lithuania) at T0, when OA was developed, and 3 months after treatment.

5.9. *Synovial fluid analyses*

Synovial fluid from both knees of each rabbit and sheep was collected to evaluate the local inflammation induced by OA through WBC and monocyte counts. Twenty μL of synovial fluid were deposited on a pre-stained slide (Testsimplets®, Waldeck) and subsequently acquired by Aperio Scanscope Digital Scanner (AT2, Leica BioSystems) at maximum resolution. Total WBC and monocyte counts were performed on each slide, taking into consideration five regions of interest of 1 mm × 1 mm on the digitalized image. ELISA cytokine determinations for IL-1β, IL-6, IL-8 and TNFα were performed on sheep synovial fluid harvested at the final endpoint of 3 months.

5.10. *Biodistribution of Titanium and Barium in rabbit organs: ICP-MS analyses*

To investigate the possible biodistribution of BaTiO₃ nanoparticles and to exclude any toxic accumulation of Titanium and Barium ICP-MS analyses were performed on blood and organ samples at the end of the long-term experimental time-point of 3 months, as well as on serial dilution of Nanocomp. Analyses were performed by Agilent 7700 ICP-MS equipped with an ASX-500 Series autosampler. MassHunter 4.2 Software by Agilent Technologies. Briefly, each sample was weighed at approximately 3 ± 0.5 g in polypropylene tubes. Subsequently, 10 mL of HNO₃ (67–69 v/v % superpure) by Carlo Erba (Cornaredo, Milano) was added and samples were mineralized at 75 °C overnight in DigiPrep SCP-Science (QuantAnalitica SRL, Osnago, Italy). The samples were then diluted with ultrapure water and filtered. Finally, before analysis by ICP-MS, the samples were further diluted with an acid solution of HNO₃ (2 %) and HCl (0.5 %). A reagent blank (HNO₃ 67–69 %) and reference sample (Matrix reference material DLA58/2016) were tested for each set of samples analyzed to ensure the reliability of results. Concentrations were calculated using a solvent calibration curve with a mixture of Ba and Ti standard solutions (CPA Chem), ranging from 0.01 to 100 ng/mL. Internal laboratory standards (Be, Ge, In, 6Li, Lu, Rh, Sc, Tb, 1 mg/L,

CPA Chem) were also continuously injected into the instrument during analysis to quantify the samples. The lower limit of quantification for Ti and Ba was set at 0.002 mg/kg.

5.11. Statistical analyses

The required rabbit sample size was estimated by an *a priori* power analysis using the G*Power v.3.1.9.2 software (Universität Kiel, Germany). Two experimental time-points (1 and 3 months) and four experimental groups were considered: 1. Untreated 2. +US, 3. Nanocomp, 4. Nanocomp +US. We hypothesized an effect $f \geq 0.40$ in histomorphometric scores in a three-way ANOVA model ('treatment', 'experimental time-point' and 'gender' factors) with $1-\beta = 0.80$ and $\alpha = 0.05$. Based on these considerations, a minimum number of $n = 96$ animals ($n = 6$ animals per group, sex and experimental time) was estimated.

Statistical analyses of data were carried out using the SPSS software (v. 29.0, IBM SPSS). Distribution normality (Shapiro–Wilk normality test) and homogeneity of variance (Levene test) were verified before data analysis. Then, data from the rabbit study were analyzed by Generalized linear mixed models with post hoc Sidak test for pairwise comparisons, considering animals and side (medial or lateral, where present) as random effects, and gender, treatment and follow-up as fixed effects. Different distributions were applied: Gamma for OARSI and Krenn scores, Multinomial for Hanashi score, Poisson for WBC counts, Tweedie for Monocyte counts and Lognormal for Safranin O score, Ca, Th, Tb, Sp and FI parameters.

Data from the sheep study were analyzed by the General Linear Model if data were normally distributed (for OARSI and Krenn scores and cartilage parameters, Gamma distribution was applied) or by Wilcoxon test followed by Monte Carlo (for Hanashi score and Monocyte count) if data were not normally distributed. Wald Chi-Squared Test was used in WBC counts and cytokine determinations in synovial fluids. Data were represented with boxplots with median, 25th and 75th percentiles and minimum and maximum, at a significance level of $p < 0.05$. Data from rabbit ASCs CD characterization and ICP-MS were analyzed by applying a paired Student *t*-test.

CRedit authorship contribution statement

Matilde Tschon: Writing – review & editing, Writing – original draft, Supervision, Resources, Methodology, Investigation, Data curation, Conceptualization. **Giorgia Codispoti:** Writing – review & editing, Writing – original draft, Visualization, Investigation, Formal analysis, Data curation. **Paolo Cabras:** Writing – review & editing, Writing – original draft, Visualization, Software, Methodology, Formal analysis, Data curation. **Andrea Cafarelli:** Writing – review & editing, Writing – original draft, Visualization, Methodology, Formal analysis, Data curation. **Diego Trucco:** Writing – review & editing, Visualization. **Lorenzo Vannozzi:** Writing – review & editing, Visualization. **Cristina Manfredini:** Writing – review & editing, Investigation, Formal analysis, Data curation. **Melania Carniato:** Writing – review & editing, Visualization, Investigation, Formal analysis, Data curation. **Giorgio Cassiolas:** Software, Formal analysis, Data curation. **Lucia Martini:** Writing – review & editing, Validation, Supervision, Resources, Investigation. **Milena Fini:** Writing – review & editing, Supervision, Conceptualization. **Giovanni D'Atri:** Formal analysis, Data curation. **Carsten Jost:** Writing – review & editing, Formal analysis. **Yirij Fedutik:** Writing – review & editing, Formal analysis. **Gilbert Daniel Nessim:** Writing – review & editing, Formal analysis. **Erik Dumont:** Writing – review & editing, Supervision. **Gina Lisignoli:** Writing – review & editing, Supervision, Data curation, Conceptualization. **Leonardo Ricotti:** Writing – review & editing, Supervision, Resources, Methodology, Funding acquisition, Conceptualization.

Funding

This work was supported by the European Union's Horizon 2020 research and innovation program, grant agreement No 814413, project ADMAIORA (ADvanced nanocomposite MAterials fOR in situ treatment and ulTRAsound-mediated management of osteoarthritis). We also acknowledge the support of the BRIEF "Biorobotics Research and Innovation Engineering Facilities" (project identification code IR0000036), a project funded under the National Recovery and Resilience Plan (NRRP), Mission 4 Component 2 Investment 3.1 of the Italian Ministry of University and Research funded by the European Union – NextGenerationEU.

Declaration of competing interest

The authors declare that they have no known competing financial interests or personal relationships that could have appeared to influence the work reported in this paper.

Acknowledgement

We are very grateful to D. Fota, L. Fergnani, S. Pellini, K. Samoggia and U. Bonanno for their technical assistance, to P. Spinnato for his help in ultrasound investigations on sheep, to E. Pignotti for her help in the statistical evaluation of *in vivo* data, to G. Fedrizzi from IZSLER – Istituto Zooprofilattico Sperimentale della Lombardia e dell'Emilia Romagna (Bologna, Italy) for ICP-MS analyses and to E. Breton from IRIS - Cube laboratory (CNRS, Université de Strasbourg) for the acquisition of the MR images of the *ex vivo* sheep specimens. We also acknowledge Andrea Aliperta for his help in the preparation of graphical abstract and figures.

Abbreviations

ACLs	Anterior cruciate ligaments
ACLT	Anterior cruciate ligaments transection
ASCs	Adipose-derived stromal cells
BTNPs	Barium titanate nanoparticles
Ca.Th	Cartilage thickness
COX-2	Cyclooxygenase-2
CT	Computed tomography
DMEM	Dulbecco's Modified Eagle Medium
D-PBS	Dulbecco's Phosphate-Buffered Saline
FBS	Fetal bovine serum
FI	Fibrillation index
FITC	Fluorescein isothiocyanate
GO	Graphene oxide
IOR	Istituto Ortopedico Rizzoli
KOA	Knee OA
LDE	long digital extensor
LIPUS	Low intensity pulsed ultrasound
M	Macrophage
MR	Magnetic resonance
Nanocomp	Nanocomposite
NSAIDs	Non-steroidal anti-inflammatory drugs
OA	Osteoarthritis
OARSI	Osteoarthritis Research Society International
PE	Phycocerythrin
ROI	Region of interest
Sbp.Th	Subchondral bone plate thickness
Tb.BV	Trabecular bone volume
Tb.N	Trabecular number
Tb.Sp	Trabecular separation
Tb.Th	Trabecular thickness
VG-RGD	VitroGel-RGD®
WBC	White blood cell
3D	3 Dimensional

Appendix A. Supplementary data

Supplementary data to this article can be found online at <https://doi.org/10.1016/j.biomaterials.2025.123728>.

Data availability

The datasets generated and analyzed during the current study are available from the corresponding author upon reasonable request.

References

- [1] K.D. Allen, L.M. Thoma, Y.M. Golightly, Epidemiology of osteoarthritis, *Osteoarthr. Cartil.* 30 (2) (2022) 184–195.
- [2] A.V. Perruccio, C. Yip, J.D. Power, M. Canizares, E.M. Badley, Examining the longitudinal associations between activity limitations, instrumental supports and social participation in osteoarthritis: a CLSA population-based study, *PLoS One* 19 (3) (2024) e0299894.
- [3] H. Long, Q. Liu, H. Yin, K. Wang, N. Diao, Y. Zhang, J. Lin, A. Guo, Prevalence trends of site-specific osteoarthritis from 1990 to 2019: findings from the global burden of disease study 2019, *Arthritis Rheumatol.* 74 (7) (2022) 1172–1183.
- [4] R.F. Loeser, S.R. Goldring, C.R. Scanzello, M.B. Goldring, Osteoarthritis: a disease of the joint as an organ, *Arthritis Rheum.* 64 (6) (2012) 1697–1707.
- [5] R. Geng, J. Li, C. Yu, C. Zhang, F. Chen, J. Chen, H. Ni, J. Wang, K. Kang, Z. Wei, Y. Xu, T. Jin, Knee osteoarthritis: current status and research progress in treatment, *Exp. Ther. Med.* 26 (4) (2023) 481 (Review).
- [6] R.R. Bannuru, M.C. Osani, E.E. Vaysbrot, N.K. Arden, K. Bennell, S.M.A. Bierma-Zeinstra, V.B. Kraus, L.S. Lohmander, J.H. Abbott, M. Bhandari, F.J. Blanco, R. Espinosa, L.K. Haugen, J. Lin, L.A. Mandl, E. Moilanen, N. Nakamura, L. Snyder-Mackler, T. Trojian, M. Underwood, T.E. McAlindon, OARSI guidelines for the non-surgical management of knee, hip, and polyarticular osteoarthritis, *Osteoarthr. Cartil.* 27 (11) (2019) 1578–1589.
- [7] G.I. Im, Y. Henrotin, Regenerative medicine for early osteoarthritis, *Ther Adv Musculoskelet Dis* 15 (2023) 1759720x231194813.
- [8] M.D. Kohn, A.A. Sassouni, N.D. Fernando, Classifications in brief: Kellgren-Lawrence classification of osteoarthritis, *Clin. Orthop. Relat. Res.* 474 (8) (2016) 1886–1893.
- [9] K.N. Malik, N. Camp, J. Chan, M. Ballard, Interventional techniques for the management of knee osteoarthritis: a literature review, *Cureus* 15 (10) (2023) e47133.
- [10] M. Maqbool, G. Fekadu, X. Jiang, F. Bekele, T. Tolossa, E. Turi, G. Fetensa, K. Fanta, An up to date on clinical prospects and management of osteoarthritis, *Ann. Med. Surg.* 72 (2021) 103077.
- [11] S. Grassel, D. Muschter, Recent advances in the treatment of osteoarthritis [version 1; peer review: 3 approved], *F1000Research* 9 (325) (2020).
- [12] R.C. Nordberg, B.J. Bielajew, T. Takahashi, S. Dai, J.C. Hu, K.A. Athanasiou, Recent advancements in cartilage tissue engineering innovation and translation, *Nat. Rev. Rheumatol.* 20 (6) (2024) 323–346.
- [13] S. Park, K.A. Rahaman, Y.-C. Kim, H. Jeon, H.-S. Han, Fostering tissue engineering and regenerative medicine to treat musculoskeletal disorders in bone and muscle, *Bioact. Mater.* 40 (2024) 345–365.
- [14] C. Manferdini, E. Gabusi, Y. Saleh, E. Lenzi, G. D'Atri, L. Ricotti, G. Lisignoli, Mesenchymal stromal cells laden in hydrogels for osteoarthritis cartilage regeneration: a systematic review from in vitro studies to clinical applications, *Cells* 11 (24) (2022).
- [15] C.G. Tabet, R.L. Pacheco, A.L.C. Martimbiano, R. Riera, A.J. Hernandez, D. F. Bueno, T.L. Fernandes, Advanced therapy with mesenchymal stromal cells for knee osteoarthritis: systematic review and meta-analysis of randomized controlled trials, *J Orthop Translat* 48 (2024) 176–189.
- [16] A. Bahari Golamkaboudi, E. Vojoudi, K. Babaeian Roshani, P. Porouhan, D. Houshang, Z. Barabadi, Current non-surgical curative regenerative therapies for knee osteoarthritis, *Stem Cell Rev Rep* 20 (8) (2024) 2104–2123.
- [17] I. Martin, J. Galipeau, C. Kessler, K. Le Blanc, F. Dazzi, Challenges for mesenchymal stromal cell therapies, *Sci. Transl. Med.* 11 (480) (2019).
- [18] M. Najar, R. Melki, F. Khalife, L. Lagneaux, F. Bouhrit, D. Moussa Agha, H. Fahmi, P. Lewalle, M. Fayyad-Kazan, M. Merimi, Therapeutic mesenchymal stem/stromal cells: value, challenges and optimization, *Front. Cell Dev. Biol.* 9 (2021) 716853.
- [19] J. Zimmermann, A.R. Farooqi, U. van Rienen, Electrical stimulation for cartilage tissue engineering - a critical review from an engineer's perspective, *Heliyon* 10 (19) (2024) e38112.
- [20] Y. Luo, M. Rahmati, A. Kazemi, W. Liu, S.W. Lee, R.M. Gyasi, G.F. López Sánchez, A. Koyanagi, L. Smith, D.K. Yon, Effects of therapeutic ultrasound in patients with knee osteoarthritis: a systematic review and meta-analysis, *Heliyon* 10 (10) (2024) e30874.
- [21] T. Wang, W. Xie, W. Ye, C. He, Effects of electromagnetic fields on osteoarthritis, *Biomed. Pharmacother.* 118 (2019) 109282.
- [22] L. Ricotti, A. Cafarelli, C. Manferdini, D. Trucco, L. Vannozzi, E. Gabusi, F. Fontana, P. Dolzani, Y. Saleh, E. Lenzi, M. Columbaro, M. Piazzzi, J. Bertacchini, A. Aliperta, M. Cain, M. Gemmi, P. Parlanti, C. Jost, Y. Fedutik, G.D. Nessim, M. Telkhozhayeva, E. Teblum, E. Dumont, C. Delbaldo, G. Codispoli, L. Martini, M. Tschon, M. Fini, G. Lisignoli, Ultrasound stimulation of piezoelectric nanocomposite hydrogels boosts chondrogenic differentiation in vitro, in both a normal and inflammatory milieu, *ACS Nano* 18 (3) (2024) 2047–2065.
- [23] F. Iacoponi, A. Cafarelli, F. Fontana, T. Pratellesi, E. Dumont, I. Barravecchia, D. Angeloni, L. Ricotti, Optimal low-intensity pulsed ultrasound stimulation for promoting anti-inflammatory effects in macrophages, *APL Bioeng.* 7 (1) (2023) 016114.
- [24] C. Rubin, M. Bolander, J.P. Ryaby, M. Hadjiargyrou, The use of low-intensity ultrasound to accelerate the healing of fractures, *J Bone Joint Surg Am* 83 (2) (2001) 259–270.
- [25] A. Cafarelli, A. Marino, L. Vannozzi, J. Puigmartí-Luis, S. Pané, G. Ciofani, L. Ricotti, Piezoelectric nanomaterials activated by ultrasound: the pathway from discovery to future clinical adoption, *ACS Nano* 15 (7) (2021) 11066–11086.
- [26] C. Paci, F. Iberite, L. Arrico, L. Vannozzi, P. Parlanti, M. Gemmi, L. Ricotti, Piezoelectric nanocomposite bioink and ultrasound stimulation modulate early skeletal myogenesis, *Biomater. Sci.* 10 (18) (2022) 5265–5283.
- [27] Y. Liu, J. Lu, Research trends of piezoelectric biomaterials in osteochondral tissue engineering, *Mater. Today Commun.* 41 (2024) 110264.
- [28] Q. Chen, Z. Zheng, M. Lin, Z. Guo, H. Huang, Q. Xue, S. Jiang, J. Wang, A. Wu, Nanocomposite hydrogels: a promising approach for the treatment of degenerative joint diseases, *Small Science* 4 (11) (2024) 2400236.
- [29] L. Ricotti, L. Vannozzi, A. Cafarelli, G.D. Nessim, G. Lisignoli, A. Wechsler, M. Eriksson, Material and System for Therapeutic Treatment of Joints, 2022. U.S. Patent Application No. 17/433,470.
- [30] J.J. Leskinen, K. Hynynen, Study of factors affecting the magnitude and nature of ultrasound exposure with in vitro set-ups, *Ultrasound Med. Biol.* 38 (5) (2012) 777–794.
- [31] W. Secomski, K. Bilmin, T. Kujawska, A. Nowicki, P. Grieb, P.A. Lewin, In vitro ultrasound experiments: standing wave and multiple reflections influence on the outcome, *Ultrasonics* 77 (2017) 203–213.
- [32] F. Fontana, F. Iberite, A. Cafarelli, A. Aliperta, G. Baldi, E. Gabusi, P. Dolzani, S. Cristino, G. Lisignoli, T. Pratellesi, E. Dumont, L. Ricotti, Development and validation of low-intensity pulsed ultrasound systems for highly controlled in vitro cell stimulation, *Ultrasonics* 116 (2021) 106495.
- [33] A. Bakhtina, M. Tohfafarosh, A. Lichtler, T.L. Arinze, Characterization and differentiation potential of rabbit mesenchymal stem cells for translational regenerative medicine, *In Vitro Cell. Dev. Biol. Anim.* 50 (3) (2014) 251–260.
- [34] H.D. Zomer, K.C. Roballo, T.B. Lessa, F.F. Bressan, N.N. Gonçalves, F.V. Meirelles, A.G. Trentin, C.E. Ambrósio, Distinct features of rabbit and human adipose-derived mesenchymal stem cells: implications for biotechnology and translational research, *Stem Cells Cloning* 11 (2018) 43–54.
- [35] X. Li, X. Lu, D. Sun, X. Wang, L. Yang, S. Zhao, H. Nian, R. Wei, Adipose-derived mesenchymal stem cells reduce lymphocytic infiltration in a rabbit model of induced autoimmune dacryoadenitis, *Investig. Ophthalmol. Vis. Sci.* 57 (13) (2016) 5161–5170.
- [36] G. Desando, I. Bartolotti, L. Cattini, M. Tschon, L. Martini, M. Fini, A. Schiavino, C. Soranzo, B. Grigolo, Prospects on the potential in vitro regenerative features of mechanically treated-adipose tissue for osteoarthritis care, *Stem Cell Rev Rep* 17 (4) (2021) 1362–1373.
- [37] M.J. Martínez-Lorenzo, M. Royo-Cañas, E. Alegre-Aguarón, P. Desportes, T. Castiella, F. García-Alvarez, L. Larrad, Phenotype and chondrogenic differentiation of mesenchymal cells from adipose tissue of different species, *J. Orthop. Res.* 27 (11) (2009) 1499–1507.
- [38] E.R. Dar, M.B. Gugjoo, M. Javaid, S. Hussain, M.R. Fazili, K. Dhama, T. Alqahtani, A.M. Alqahtani, R.A. Shah, T.B. Emran, Adipose Tissue- and bone marrow-derived mesenchymal stem cells from sheep: culture characteristics, *Animals (Basel)* 11 (8) (2021).
- [39] T. Ruediger, V. Horbert, A. Reuther, P. Kumar Kalla, R.H. Burgkart, M. Walther, R.W. Kinne, J. Mika, Thickness of the stifle joint articular cartilage in different large animal models of cartilage repair and regeneration, *Cartilage* 13 (2,suppl) (2021) 438s–452s.
- [40] T. Oláh, J.C. Michaelis, X. Cai, M. Cucchiari, H. Madry, Comparative anatomy and morphology of the knee in translational models for articular cartilage disorders. Part II: small animals, *Ann. Anat.* 234 (2021) 151630.
- [41] J. Patel, S. Chen, T. Katzmeyer, Y.A. Pei, M. Pei, Sex-dependent variation in cartilage adaptation: from degeneration to regeneration, *Biol. Sex Differ.* 14 (1) (2023) 17.
- [42] G. Filardo, E. Kon, L. Andriolo, F. Vannini, R. Buda, A. Ferruzzi, S. Giannini, M. Marcacci, Does patient sex influence cartilage surgery outcome? Analysis of results at 5-year follow-up in a large cohort of patients treated with matrix-assisted autologous chondrocyte transplantation, *Am. J. Sports Med.* 41 (8) (2013) 1827–1834.
- [43] N.A. Segal, J.M. Nilges, W.M. Oo, Sex differences in osteoarthritis prevalence, pain perception, physical function and therapeutics, *Osteoarthr. Cartil.* 32 (9) (2024) 1045–1053.
- [44] H.L. Stewart, D. Gilbert, D. Stefanovski, Z. Garman, M.B. Albro, M. Bais, M. W. Grinstaff, B.D. Snyder, T.P. Schaer, A missed opportunity: a scoping review of the effect of sex and age on osteoarthritis using large animal models, *Osteoarthr. Cartil.* 32 (5) (2024) 501–513.
- [45] M. Tschon, D. Contartese, S. Pagani, V. Borsari, M. Fini, Gender and sex are key determinants in osteoarthritis not only confounding variables. A systematic review of clinical data, *J. Clin. Med.* 10 (14) (2021).
- [46] D. Contartese, M. Tschon, M. De Mattei, M. Fini, Sex specific determinants in osteoarthritis: a systematic review of preclinical studies, *Int. J. Mol. Sci.* 21 (10) (2020).

- [47] M. Buoncervello, M. Marconi, A. Carè, P. Piscopo, W. Malorni, P. Matarrese, Preclinical models in the study of sex differences, *Clin. Sci. (Lond.)* 131 (6) (2017) 449–469.
- [48] B. Phillips, T.N. Haschler, N.A. Karp, Including both sexes in in vivo research does not necessitate an increase in sample size: a key role for factorial analysis methods, *bioRxiv* (2022), 2022.09.29.510061.
- [49] D. Hanashi, T. Koshino, M. Uesugi, T. Saito, Effect of femoral nerve resection on progression of cartilage degeneration induced by anterior cruciate ligament transection in rabbits, *J. Orthop. Sci.* 7 (6) (2002) 672–676.
- [50] S. Laverty, C.A. Girard, J.M. Williams, E.B. Hunziker, K.P. Pritzker, The OARSI histopathology initiative - recommendations for histological assessments of osteoarthritis in the rabbit, *Osteoarthr. Cartil.* 18 (2010) S53–S65. Suppl. 3.
- [51] G. Tiralocche, C. Girard, L. Chouinard, J. Sampalis, L. Moquin, M. Ionescu, A. Reiner, A.R. Poole, S. Laverty, Effect of oral glucosamine on cartilage degradation in a rabbit model of osteoarthritis, *Arthritis Rheum.* 52 (4) (2005) 1118–1128.
- [52] G. Desando, M. Tschon, L. Martini, M. Sartori, G. Giavaresi, M. Fini, A. Cellamare, C. Soranzo, C. Longinotti, M. D'Alessandro, L. Roseti, B. Grigolo, 3D connective micro-fragment enriched with stromal vascular fraction in osteoarthritis: chondroprotective evidence in a preclinical in vivo model, *Front. Cell Dev. Biol.* 13 (2025) 1533405.
- [53] M. Li, M. Hao, D. Jiang, Y. Chen, W. Wang, In vivo tracking of human adipose-derived mesenchymal stem cells in a rat knee Osteoarthritis model with fluorescent lipophilic membrane dye, *J. Vis. Exp.* 128 (2017).
- [54] M. Li, X. Luo, X. Lv, V. Liu, G. Zhao, X. Zhang, W. Cao, R. Wang, W. Wang, In vivo human adipose-derived mesenchymal stem cell tracking after intra-articular delivery in a rat osteoarthritis model, *Stem Cell Res. Ther.* 7 (1) (2016) 160.
- [55] Q. Pang, J. Zhan, Z. Chen, L. Dong, W. Huang, Emerging therapy in osteoarthritis: mesenchymal stem cells, secretomes, and using hydrogels to enhance efficacy, *BioDrugs* 39 (4) (2025) 555–571.
- [56] H.H. Alfaqeh, R.B.H. Idrus, A.B. Saim, A. Nordin, Synergistic effects of natural products and mesenchymal stem cells in osteoarthritis treatment: a narrative review, *Curr. Issues Mol. Biol.* 47 (6) (2025).
- [57] M. Mahmoud, M. Abdel-Rasheed, R.E. Galal, R.R. El-Awady, Factors defining human adipose stem/stromal cell immunomodulation in vitro, *Stem Cell Rev Rep* 20 (1) (2024) 175–205.
- [58] L. Zenic, D. Polancec, D. Hudetz, Z. Jelec, E. Rod, D. Vidovic, M. Staresinic, S. Sabalic, T. Vrdoljak, T. Petrovic, F. Cukelj, V. Molnar, M. Cemerin, V. Maticic, P. Brlek, Z. Djukic Koroljevic, I. Boric, G. Lauc, D. Primorac, Polychromatic flow cytometric analysis of stromal vascular fraction from liposarcoma and microfragmented counterparts reveals sex-related immunophenotype differences, *Genes* 12 (12) (2021).
- [59] K.E. Knewton, N.R. Ohl, J.L. Robinson, Estrogen signaling dictates musculoskeletal stem cell behavior: sex differences in tissue repair, *Tissue Eng Part B Rev* 28 (4) (2022) 789–812.
- [60] E. Bianconi, R. Casadei, F. Frabetti, C. Ventura, F. Facchin, S. Canaider, Sex-specific transcriptome differences in human adipose mesenchymal stem cells, *Genes* 11 (8) (2020).
- [61] G. Maged, M.A. Abdelsamed, H. Wang, A. Lotfy, The potency of mesenchymal stem/stromal cells: does donor sex matter? *Stem Cell Res. Ther.* 15 (1) (2024) 112.
- [62] C. Delbaldo, M. Tschon, L. Martini, M. Fini, G. Codispoti, Benefits of applying nanotechnologies to hydrogels in efficacy tests in Osteoarthritis Models-A systematic review of preclinical studies, *Int. J. Mol. Sci.* 23 (15) (2022).
- [63] Y. Liu, G. Dzditor, T.T. Le, T. Vinikoor, K. Morgan, E.J. Curry, R. Das, A. McClinton, E. Eisenberg, L.N. Apuzzo, K.T.M. Tran, P. Prasad, T.J. Flanagan, S. W. Lee, H.M. Kan, M.T. Chorsi, K.W.H. Lo, C.T. Laurencin, T.D. Nguyen, Exercise-induced piezoelectric stimulation for cartilage regeneration in rabbits, *Sci. Transl. Med.* 14 (627) (2022) eabi7282.
- [64] T. Vinikoor, G.K. Dzditor, T.T. Le, Y. Liu, H.M. Kan, S. Barui, M.T. Chorsi, E. J. Curry, E. Reinhardt, H. Wang, P. Singh, M.A. Merriman, E. D'Orio, J. Park, S. Xiao, J.H. Chapman, F. Lin, C.S. Truong, S. Prasad, L. Chuba, S. Killoh, S. W. Lee, Q. Wu, R.M. Chidambaram, K.W.H. Lo, C.T. Laurencin, T.D. Nguyen, Injectable and biodegradable piezoelectric hydrogel for osteoarthritis treatment, *Nat. Commun.* 14 (1) (2023) 6257.
- [65] D. Wang, Y. Zhang, L. Zhang, D. He, L. Zhao, Z. Miao, W. Cheng, C. Zhu, L. Zhu, W. Zhang, H. Jin, H. Zhu, H. Pan, IRF1 governs the expression of SMARCC1 via the GCN5-SETD2 axis and actively engages in the advancement of osteoarthritis, *J Orthop Translat* 45 (2024) 211–225.
- [66] T.M. Griffin, C.R. Scanzello, Innate inflammation and synovial macrophages in osteoarthritis pathophysiology, *Clin. Exp. Rheumatol.* 37 (2019) 57–63. Suppl 120(5).
- [67] C. Zhu, S. Han, X. Zeng, C. Zhu, Y. Pu, Y. Sun, Multifunctional thermo-sensitive hydrogel for modulating the microenvironment in Osteoarthritis by polarizing macrophages and scavenging ROS, *J. Nanobiotechnol.* 20 (1) (2022) 221.
- [68] S. Ravi, L.P.P. Chokkakula, S.R. Dey, S.N. Rath, Fabrication of hypoxia-mimicking supramolecular hydrogels for cartilage repair, *ACS Appl. Bio Mater.* 8 (2) (2025) 1261–1277.
- [69] L. Zhang, X. Chen, P. Cai, H. Sun, S. Shen, B. Guo, Q. Jiang, Reprogramming mitochondrial metabolism in synovial macrophages of early osteoarthritis by a camouflaged meta-defensome, *Adv Mater* 34 (30) (2022) e2202715.
- [70] H. Wei, H. Huang, H. He, Y. Xiao, L. Chun, Z. Jin, H. Li, L. Zheng, J. Zhao, Z. Qin, Pt-Se hybrid nanozymes with potent catalytic activities to scavenge ROS/RONS and regulate macrophage polarization for osteoarthritis therapy, *Research* 7 (2024) 310.
- [71] Z. Qin, X. Li, P. Wang, Q. Liu, Y. Li, A. Gu, Q. Jiang, N. Gu, Ultrasmall prussian blue nanozyme attenuates osteoarthritis by scavenging reactive oxygen species and regulating macrophage phenotype, *Nano Lett.* 24 (37) (2024) 11697–11705.
- [72] J. Liu, Z. Liu, Y. Pang, H. Zhou, The interaction between nanoparticles and immune system: application in the treatment of inflammatory diseases, *J Nanobiotechnol* 20 (1) (2022) 127.
- [73] P. Wu, L. Shen, H.F. Liu, X.H. Zou, J. Zhao, Y. Huang, Y.F. Zhu, Z.Y. Li, C. Xu, L. H. Luo, Z.Q. Luo, M.H. Wu, L. Cai, X.K. Li, Z.G. Wang, The marriage of immunomodulatory, angiogenic, and osteogenic capabilities in a piezoelectric hydrogel tissue engineering scaffold for military medicine, *Mil Med Res* 10 (1) (2023) 35.
- [74] H. Wu, H. Dong, Z. Tang, Y. Chen, Y. Liu, M. Wang, X. Wei, N. Wang, S. Bao, D. Yu, Z. Wu, Z. Yang, X. Li, Z. Guo, L. Shi, Electrical stimulation of piezoelectric BaTiO₃ coated Ti6Al4V scaffolds promotes anti-inflammatory polarization of macrophages and bone repair via MAPK/JNK inhibition and OXPHOS activation, *Biomaterials* 293 (2023) 121990.
- [75] W.S. Cho, B.C. Kang, J.K. Lee, J. Jeong, J.H. Che, S.H. Seok, Comparative absorption, distribution, and excretion of titanium dioxide and zinc oxide nanoparticles after repeated oral administration, *Part. Fibre Toxicol.* 10 (2013) 9.
- [76] L. Geraets, A.G. Oomen, P. Krystek, N.R. Jacobsen, H. Wallin, M. Laurentie, H. W. Verharen, E.F. Brandon, W.H. de Jong, Tissue distribution and elimination after oral and intravenous administration of different titanium dioxide nanoparticles in rats, *Part. Fibre Toxicol.* 11 (2014) 30.
- [77] G. Graziani, D. Ghezzi, M. Boi, N. Baldini, E. Sassoni, M. Cappelletti, G. Fedrizzi, M. Maglio, F. Salamanna, M. Tschon, L. Martini, S. Zaffagnini, M. Fini, M. Sartori, Ionized jet deposition of silver nanostructured coatings: assessment of chemico-physical and biological behavior for application in orthopedics, *Biomater. Adv.* 159 (2024) 213815.
- [78] J. Geurts, F. Andrey, J. Favre, T. Hügle, P. Omoumi, Morphological and histological features of thicker cartilage at the posterior medial femoral condyle in advanced knee osteoarthritis, *Osteoarthr Cartil Open* 6 (3) (2024) 100502.
- [79] S. Cotofana, R. Buck, W. Wirth, F. Roemer, J. Duryea, M. Nevitt, F. Eckstein, Cartilage thickening in early radiographic knee osteoarthritis: a within-person, between-knee comparison, *Arthritis Care Res.* 64 (11) (2012) 1681–1690.
- [80] E. Calvo, I. Palacios, E. Delgado, O. Sánchez-Pernaute, R. Largo, J. Egido, G. Herrero-Beaumont, Histopathological correlation of cartilage swelling detected by magnetic resonance imaging in early experimental osteoarthritis, *Osteoarthr. Cartil.* 12 (11) (2004) 878–886.
- [81] E. Calvo, I. Palacios, E. Delgado, J. Ruiz-Cabello, P. Hernández, O. Sánchez-Pernaute, J. Egido, G. Herrero-Beaumont, High-resolution MRI detects cartilage swelling at the early stages of experimental osteoarthritis, *Osteoarthr. Cartil.* 9 (5) (2001) 463–472.
- [82] P. Vahedi, H. Hosainzadegan, B. Brazvan, L. Roshangar, H. Shafaei, R. Salimejad, Treatment of cartilage defects by low-intensity pulsed ultrasound in a sheep model, *Cell Tissue Bank.* 22 (3) (2021) 369–378.
- [83] C. Feng, X. Luo, N. He, H. Xia, X. Lv, X. Zhang, D. Li, F. Wang, J. He, L. Zhang, X. Lin, L. Lin, H. Yin, J. He, J. Wang, W. Cao, R. Wang, G. Zhou, W. Wang, Efficacy and persistence of allogeneic adipose-derived mesenchymal stem cells combined with hyaluronic acid in osteoarthritis after intra-articular injection in a sheep model, *Tissue Eng Part A* 24 (3–4) (2018) 219–233.
- [84] X. Lv, J. He, X. Zhang, X. Luo, N. He, Z. Sun, H. Xia, V. Liu, L. Zhang, X. Lin, L. Lin, H. Yin, D. Jiang, W. Cao, R. Wang, G. Zhou, W. Wang, Comparative efficacy of autologous stromal vascular fraction and autologous adipose-derived mesenchymal stem cells combined with hyaluronic acid for the treatment of sheep osteoarthritis, *Cell Transplant.* 27 (7) (2018) 1111–1125.
- [85] F. Veronesi, M. Fini, L. Martini, P. Berardinelli, V. Russo, G. Filardo, B. Di Matteo, M. Marcacci, E. Kon, In vivo model of osteoarthritis to compare allogenic amniotic epithelial stem cells and autologous adipose derived cells, *Biology* 11 (5) (2022).
- [86] R.C. Appleyard, P. Ghosh, M.V. Swain, Biomechanical, histological and immunohistological studies of patellar cartilage in an ovine model of osteoarthritis induced by lateral meniscectomy, *Osteoarthr. Cartil.* 7 (3) (1999) 281–294.
- [87] C. Little, S. Smith, P. Ghosh, C. Bellenger, Histomorphological and immunohistochemical evaluation of joint changes in a model of osteoarthritis induced by lateral meniscectomy in sheep, *J. Rheumatol.* 24 (11) (1997) 2199–2209.
- [88] M.A. Cake, R.A. Read, G. Corfield, A. Daniel, D. Burkhardt, M.M. Smith, C. B. Little, Comparison of gait and pathology outcomes of three meniscal procedures for induction of knee osteoarthritis in sheep, *Osteoarthr. Cartil.* 21 (1) (2013) 226–236.
- [89] G. Filardo, M. Tschon, F. Perdisa, S. Brogini, C. Cavallo, G. Desando, G. Giavaresi, B. Grigolo, L. Martini, N. Nicoli Aldini, A. Roffi, M. Fini, E. Kon, Micro-fragmentation is a valid alternative to cell expansion and enzymatic digestion of adipose tissue for the treatment of knee osteoarthritis: a comparative preclinical study, *Knee Surg. Sports Traumatol. Arthrosc.* 30 (3) (2022) 773–781.
- [90] G. Desando, C. Cavallo, M. Tschon, G. Giavaresi, L. Martini, M. Fini, R. Giardino, A. Facchini, B. Grigolo, Early-term effect of adult chondrocyte transplantation in an osteoarthritis animal model, *Tissue Eng Part A* 18 (15–16) (2012) 1617–1627.
- [91] C.B. Little, M.M. Smith, M.A. Cake, R.A. Read, M.J. Murphy, F.P. Barry, The OARSI histopathology initiative - recommendations for histological assessments of osteoarthritis in sheep and goats, *Osteoarthr. Cartil.* 18 (2010) S80–S92. Suppl 3.
- [92] K.I. Barton, M. Shekarforoush, B.J. Heard, J.L. Sevcik, P. Vakil, M. Atarod, R. Martin, Y. Achari, D.A. Hart, C.B. Frank, N.G. Shrive, Use of pre-clinical

- surgically induced models to understand biomechanical and biological consequences of PTOA development, *J. Orthop. Res.* 35 (3) (2017) 454–465.
- [93] H. Dou, S. Wang, J. Hu, J. Song, C. Zhang, J. Wang, L. Xiao, Osteoarthritis models: from animals to tissue engineering, *J. Tissue Eng.* 14 (2023) 20417314231172584.
- [94] B.E. Treeby, B.T. Cox, k-Wave: MATLAB toolbox for the simulation and reconstruction of photoacoustic wave fields, *J. Biomed. Opt.* 15 (2) (2010) 021314.
- [95] A. Fedorov, R. Beichel, J. Kalpathy-Cramer, J. Finet, J.C. Fillion-Robin, S. Pujol, C. Bauer, D. Jennings, F. Fennessy, M. Sonka, J. Buatti, S. Aylward, J.V. Miller, S. Pieper, R. Kikinis, 3D slicer as an image computing platform for the quantitative imaging Network, *Magn. Reson. Imaging* 30 (9) (2012) 1323–1341.
- [96] P.A. Hasgall, F. Di Gennaro, C. Baumgartner, E. Neufeld, B. Lloyd, M.C. Gosselin, N. Kuster, Available online, Version 4.1, 2022. <https://itis.swiss/virtual-population/tissue-properties/database/dielectric-properties..ITISDatabaseforThermalandElectromagneticParametersofBiologicalTissues>.
- [97] A. Cafarelli, A. Verbeni, A. Poliziani, P. Dario, A. Menciassi, L. Ricotti, Tuning acoustic and mechanical properties of materials for ultrasound phantoms and smart substrates for cell cultures, *Acta Biomater.* 49 (2017) 368–378.
- [98] A.J. Smith, R.E. Clutton, E. Lilley, K.E.A. Hansen, T. Brattelid, PREPARE: guidelines for planning animal research and testing, *Lab Anim* 52 (2) (2018) 135–141.
- [99] N. Percie du Sert, A. Ahluwalia, S. Alam, M.T. Avey, M. Baker, W.J. Browne, A. Clark, I.C. Cuthill, U. Dirnagl, M. Emerson, P. Garner, S.T. Holgate, D. W. Howells, V. Hurst, N.A. Karp, S.E. Lazic, K. Lidster, C.J. MacCallum, M. Macleod, E.J. Pearl, O.H. Petersen, F. Rawle, P. Reynolds, K. Rooney, E. S. Sena, S.D. Silberberg, T. Steckler, H. Würbel, Reporting animal research: explanation and elaboration for the ARRIVE guidelines 2.0, *PLoS Biol.* 18 (7) (2020) e3000411.
- [100] C. Häger, S. Biernot, M. Buettner, S. Glage, L.M. Keubler, N. Held, E.M. Bleich, K. Otto, C.W. Müller, S. Decker, S.R. Talbot, A. Bleich, The Sheep grimace scale as an indicator of post-operative distress and pain in laboratory sheep, *PLoS One* 12 (4) (2017) e0175839.
- [101] F. Veronesi, F. Vandenbulcke, K. Ashmore, B. Di Matteo, N. Nicoli Aldini, L. Martini, M. Fini, E. Kon, Meniscectomy-induced osteoarthritis in the sheep model for the investigation of therapeutic strategies: a systematic review, *Int. Orthop.* 44 (4) (2020) 779–793.
- [102] A. Mahajan, S. Hazra, A. Arora, D.S. Katti, Isolation, expansion, and differentiation of mesenchymal stem cells from the infrapatellar fat pad of the goat stifle joint, *J. Vis. Exp.* 186 (2022).
- [103] V. Krenn, L. Morawietz, G.R. Burmester, R.W. Kinne, U. Mueller-Ladner, B. Muller, T. Haupt, Synovitis score: discrimination between chronic low-grade and high-grade synovitis, *Histopathology* 49 (4) (2006) 358–364.
- [104] K.P. Pritzker, S. Gay, S.A. Jimenez, K. Ostergaard, J.P. Pelletier, P.A. Revell, D. Salter, W.B. van den Berg, Osteoarthritis cartilage histopathology: grading and staging, *Osteoarthr. Cartil.* 14 (1) (2006) 13–29.